EPA-600/7-80-018

January 1980

A Theoretical Analysis of Nitric Oxide Production in a Methane/Air Turbulent Diffusion Flame

by

Frank E. Marble (California Institute of Technology)
and James E. Broadwell

TRW Defense and Space Systems Group
One Space Park
Redondo Beach, California 90278

Contract No. 68-02-2613
Program Element No. INE829

EPA Project Officer: W.S. Lanier

Industrial Environmental Research Laboratory
Office of Environmental Engineering and Technology
Research Triangle Park, NC 27711

Prepared for

U.S. ENVIRONMENTAL PROTECTION AGENCY
Office of Research and Development
Washington, DC 20460

ABSTRACT

The coherent flame model is applied to the methane-air turbulent diffusion flame with the objective of describing the production of nitric oxide. The example of a circular jet of methane discharging into a stationary air atmosphere is used to illustrate application of the model. In the model, the chemical reactions take place in laminar flame elements which are lengthened by the turbulent fluid motion and shortened when adjacent flame segments consume intervening reactant. The rates with which methane and air are consumed and nitric oxide generated in the strained laminar flame are computed numerically in an independent calculation.

The model predicts nitric oxide levels of approximately 80 parts per million at the end of the flame generated by a 30.5 cm (1 foot) diameter jet of methane issuing at 3.05×10^3 cm/sec (100 ft/sec). The model also predicts that this level varies directly with the fuel jet diameter and inversely with the jet velocity.

A possibly important nitric oxide production mechanism, neglected in the present analysis, can be treated in a proposed extension to the model.

CONTENTS

LIST OF FIGURES

LIST OF TABLES

ACKNOWLEDGEMENT

The authors wish to acknowledge an essential contribution of the technical staff of the Energy and Environmental Research Corporation to this work.

I. CONCLUSIONS

A theoretical model of a turbulent diffusion flame has been developed and applied to a methane jet burning in air. The model predicts nitric oxide levels of approximately 80 parts per million at the end of the flame generated by a 30.5 cm (1 foot) diameter jet of methane issuing at 3.05×10^3 cm/sec (100 ft/sec). In the model this level varies directly with the fuel jet diameter and inversely with the jet velocity. A possibly important nitric oxide production mechanism, neglected in the present analysis, can be treated in a proposed extension to the model.

II. RECOMMENDATIONS

Additional experimental data describing nitric oxide production in turbulent methane-air flames of different dimensions is needed to assist in the establishment of the scaling laws. Such data would also allow a critical assessment of the present state of the coherent flame model and guide its further development. It is recommended that such experiments and the proposed extension of the model be carried out.

III. INTRODUCTION

The coherent flame front model[1] is a description of fast chemical reactions in turbulent flow in which the reactions are assumed confined to thin flame surfaces. The turbulent flame structure then consists of a distribution of these surface elements. The model describes the manner in which the flame elements are stretched and dispersed by the turbulent motion, as well as the mechanism by which neighboring flame surfaces consume the intervening reactant and annihilate each other. These processes are shown schematically in Figure 1. A considerable advantage of the coherent flame model is that it effectively separates the detailed structure of the laminar flames from the fluid mechanics so that systems with complex chemical reactions may be treated nearly as easily as simple ones.

The work to be described here treats the methane-air flame and the attendant production of nitric oxide. The individual flame surfaces have internal distributions of temperature and reactants that favor the production of nitric oxide. The nitric oxide so produced diffuses back out of the heat zone into the cooler portions of the flame surface structure. The production then appears as that stored in the flame surface as well as that deposited in the products resulting from flame annihilation.

Now it is clear that the mechanism described above neglects the nitric oxide produced "in the bulk" which, in the present picture, consists of the products resulting from flame annihilation, slowly mixing with unconsumed reactants. The additional production is of two parts: 1) that generated in the products and 2) that generated in flames supported by reactants contaminated by combustion products. In the following work, an effort has been made to account for the second of these, that due to "re-processing" the reaction products. The first requires a major effort to account properly for this mechanism and, while an outline of the proposed technique is given, no implementation of calculations have been performed.

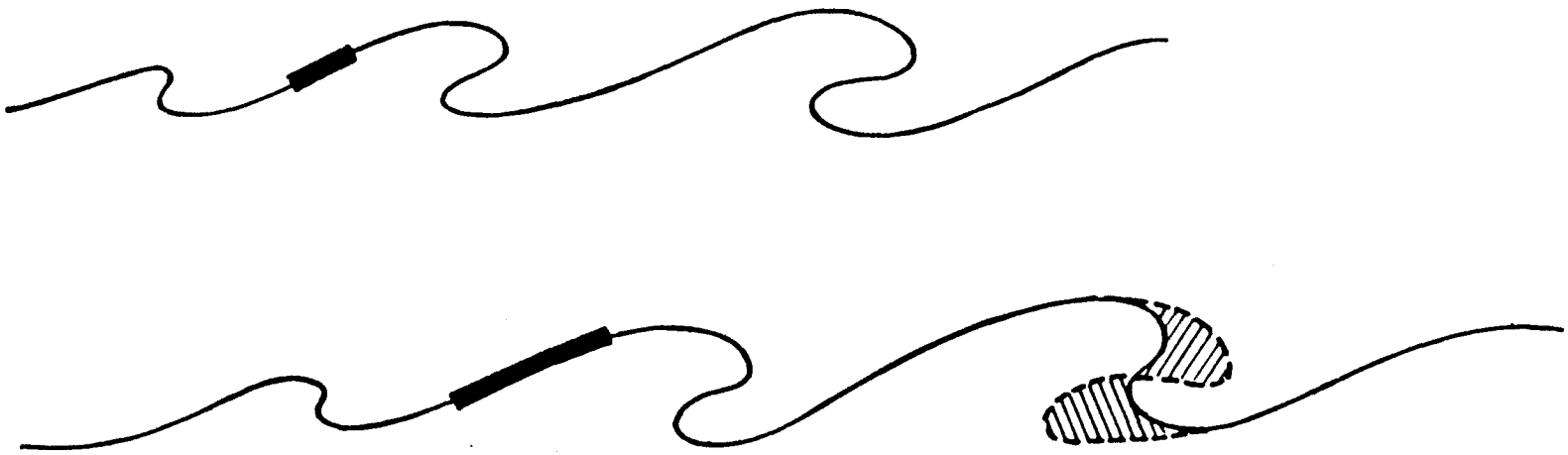

1. SURFACE STRETCHING
2. TURBULENT TRANSPORT
3. MUTUAL ANNIHILATION

Figure 1. Elements of coherent flame model

IV. THE FLAME STRUCTURE MODEL

For purpose of this analysis, the turbulent flame is assumed to consist of a distribution of laminar diffusion flame elements. The fuel and oxidizer, which exist on one or the other side of the flame element, are either the pure gases -- the injected fuel and the ambient oxidizer -- or fuel and oxidizer that has been diluted by thorough mixing with combustion products.

To make this picture quantitative, we define the flame surface density Σ to be the flame surface area per unit volume. Both in this concept and in the assumptions of the flame elements, the dimensions of the flame surface are very large in comparison with its thickness, so that the characterization of the structure by the flame surface area is reasonable. The local flame surface density is altered by three processes: 1) flame surface production resulting from fluid straining motions in the plane of the flame, 2) turbulent transport by which flame elements are carried from one region of the fluid to another by large scale turbulent fluctuations, and 3) flame annihilation, in which flame surfaces consume the intervening fuel or oxidizer with the result that these flame surfaces vanish.

The flame surface elements that are involved in this representation are not the usual laminar diffusion flame structures, but are dominated by the straining motions of the reactants in the plane of the flame. In this circumstance, the structure of the flame is no longer time-dependent, but is fixed by the local straining rate of the fluid. Then $\varepsilon \sim 1/\text{time}$ is the straining rate, and $D \sim (\text{length})^2/\text{time}$ is the molecular diffusion coefficient, then the flame assumes a local thickness $\sim \sqrt{D/\varepsilon}$ and consumes reactants at a volumetric rate $\sim \sqrt{D\varepsilon}$ per unit flame surface area. If the strain rate ε varies from point to point in the turbulent region, or varies with time as one follows the fluid mass, then the flame will be assumed to vary its structure in a quasi-steady manner. This theory of time-dependent diffusion flames in a straining gas motion is given in appendix A.

When the flame surface density Σ and the strain rate ϵ are known locally, the reactant consumption rates within this region are known also because they are fixed by the flame structure. The actual flame structure may be calculated to any degree of approximation between the simplest, where the chemical reaction rates are very rapid so that the reactant consumption is controlled by molecular diffusion, to the detailed structure involving the complete chemistry with appropriate rates. The flame structure with finite rates requires numerical calculation but, because it is a steady one-dimensional problem, the actual calculations may be accomplished with relative ease.

The appropriate form of the equation describing the flame surface density may be deduced from first principles by considering the distortion and migration of surface elements, fixed to the fluid, in a turbulent medium.[2] Here, it will be sufficient to motivate the form by physical reasoning and then to suggest the manner in which the various terms scale with features of the flowfield and the chemistry of the flame structure. Now in a fluid with mean velocity components U_i, the expression

$$\frac{D\Sigma}{Dt} \equiv \frac{\partial \Sigma}{\partial t} + U_j \frac{\partial \Sigma}{\partial x_j}$$

gives the change in flame density following a mean fluid element. According to our model described earlier, this change may be written in the following form

$\frac{D\Sigma}{Dt}$ = turbulent diffusion of flame surface into the region

+ increase of individual surface element area by turbulent straining motions

- reduction in flame surface resulting from local consumption of one of the reactants.

In these calculations, the turbulent diffusion of flame surface will be described using a turbulent diffusivity and the assumption that the

turbulent fluctuation velocities are large in comparison with molecular diffusion velocities, familiar from usual turbulent treatments of heat and mass transport. Thus, if we donote **D** the turbulent diffusion coefficient that arises in the description of momentum exchange, the turbulent diffusion term applicable to the treatment of the turbulent circular jet, which we treat as our example, is

$$\frac{1}{r}\frac{\partial}{\partial r}\left(r\,\mathbf{D}\,\frac{\partial \Sigma}{\partial r}\right)$$

where the appropriate boundary layer approximation has been made. The rate of increase of an element of flame surface area is proportional to the strain rate in the turbulent fluctuations. Under the assumption that this strain rate is proportional to the rate of strain in the mean motions, the rate of increase in flame surface density is thus proportional to the product of the strain rate of mean motion and the local flame density. Then, calling α the unknown constant of proportionality, we take the second term on the right equal to

$$\varepsilon\ \Sigma\ \equiv\ \alpha\left|\frac{\partial W}{\partial r}\right|\ \Sigma$$

where, again, we have written the term in the form appropriate to the circular jet, W being the velocity component of the mean motion in the direction of the symmetry axis.

The general nature of the process by which flame surface is removed from the field is best pictured by considering two neighboring laminar diffusion flame fronts parallel to each other and containing one constituent, say, fuel, between them. As the motion progresses, the intervening fuel is consumed and both elements of flame surface are extinguished. A similar process takes place if the intervening constituent is the oxidizer. To make the mechanism quantitative consider a volume containing many flame elements. The fraction of local volume occupied by fuel is proportional, under our assumption of constant density, to the mass fraction κ_1 of fuel. Moreover, the rates of reactant consumption by an element of laminar flame are presumed known from detailed calculations of that flame structure. If we call v_1 the volume rate of consumption of fuel per unit flame area, the rate at which volume occupied by fuel is being consumed in a unit volume of space is $v_1\ \Sigma$.

But that unit volume of space contains only a fraction κ_1 of fuel so that the rate of fuel consumption in a unit volume of space divided by the amount of fuel contained in that volume is $v_i \Sigma/\kappa_1$. Thus, if the flame surface area is nearly uniformly distributed over the region, this expression gives also the fractional rate of flame surface annihilation so that the flame surface area reduction rate due to fuel consumption is

$$\left(v_i \Sigma/\kappa_1\right) \Sigma = \frac{v_1}{\kappa_1} \Sigma^2$$

In a completely similar manner, we may reason that the flame surface area reduction due to consumption of oxidizer is proportional to

$$\frac{v_2}{\kappa_2} \Sigma^2$$

and because in a given region, individual surface elements are being removed by either the exhaustion of fuel or of oxidizer, the two expressions will be considered independent and additive.

If now we collect the various terms that have been discussed, it is possible to write in detail the conservation equations for flame surface density

$$U \frac{\partial \Sigma}{\partial r} + W \frac{\partial \Sigma}{\partial z} = \frac{1}{r} \frac{\partial}{\partial r} \left(r \mathbf{D} \frac{\partial \Sigma}{\partial r} \right) + \varepsilon \Sigma - \lambda \frac{v_1}{\kappa_1} \Sigma^2 - \lambda \frac{v_2}{\kappa_2} \Sigma^2 \qquad (1)$$

The form of equation has been chosen to be that appropriate for the analysis of the circular jet.

The conservation equations for the individual species are conventional except for the terms describing the reactant consumption by chemical reaction. These will be given in terms of the flame surface density and the reactant consumption for a unit flame surface supplied by one-dimensional flame calculations. For the fast chemical reaction, we need consider only three constituents, the fuel κ_1, the oxidizer κ_2, and the product κ_3, related by the fact that the sum of mass fractions is unity

$$\kappa_1 + \kappa_2 + \kappa_3 = 1 \qquad (2)$$

so that only two of these, κ_1 and κ_2, need be treated in detail. The actual chemistry, in contrast to the overall reaction between fuel and oxidizer, is contained within the one-dimensional flame structure.

The consumption rate of fuel per unit volume is simply the product of the effective influx velocity v_1, the flame surface density Σ, and the mass fraction κ_1^* of fuel in the fuel-containing constituent of the turbulent structure. The conservation equation for fuel may be written down directly as

$$U \frac{\partial \kappa_1}{\partial r} + W \frac{\partial \kappa_1}{\partial z} = \frac{1}{r} \frac{\partial}{\partial r} \left(r D \frac{\partial \kappa_1}{\partial r} \right) - \kappa_1^* v_1 \Sigma \tag{3}$$

Similarly, the conservation equation for the oxidizer component is

$$U \frac{\partial \kappa_2}{\partial r} + W \frac{\partial \kappa_2}{\partial z} = \frac{1}{r} \frac{\partial}{\partial r} \left(r D \frac{\partial \kappa_2}{\partial r} \right) - \kappa_2^* v_2 \Sigma \tag{4}$$

It remains to define the consumption rates v_1 and v_2 for the fuel and oxidizer components. Regardless of whether these quantities are defined through use of infinitely fast reaction rates or by detailed calculation of the one-dimensional flame structure, they depend upon the reactant concentrations on each side of the flame, κ_1 and κ_2, and the local strain rate ε of the mean flow. It is this latter item which couples the local diffusion flame structure to the gasdynamic structure.

V. THE TURBULENT CIRCULAR FUEL JET

The detailed solution for a turbulent flame structure described in the manner outlined in the previous section requires a turbulence model for the mean flow and, because there is a choice of turbulence model to be used, it is preferable to go directly to the example of interest rather than describe the procedure in general. For the problem of the circular fuel jet, we shall choose the elementary model utilizing a scalar turbulent diffusivity. Furthermore, we shall, in the interests of simplicity, neglect the change of mean gas density associated with the chemical reactions. This restriction in no way implies that the density change is a negligible factor. Rather the use of a turbulence model for flows of non-uniform density introduces a degree of uncertainty of its own which makes it additionally difficult to judge the merits of the flame model.

Under these restrictions, the gasdynamic field is described by the equations

$$\frac{1}{r}\frac{\partial}{\partial r}(rU) + \frac{\partial W}{\partial z} = 0 \tag{5}$$

$$U\frac{\partial W}{\partial r} + W\frac{\partial W}{\partial z} = \frac{1}{r}\frac{\partial}{\partial r}\left(r\frac{\tau_{rz}}{\rho}\right) \tag{6}$$

where the pressure of the far field has been assumed constant. Using the eddy-diffusivity model for the turbulent shear stress τ_{rz}, we write

$$\frac{\tau_{rz}}{\rho} = \mathbf{D}\frac{\partial W}{\partial r} \tag{7}$$

where $\mathbf{D}$ is the turbulent analogue to the kinematic viscosity. The customary difficulty arises here in the choice, rather than the determination, of the eddy diffusivity. For the circular jet, however, the choice is made simpler by the fact that the jet momentum, which is conserved along the direction of

flow, has the dimension of $(\text{velocity})^2 \times (\text{length})^2$. And because **D** has the dimension of (length) x (velocity), there being no other characteristic dimensions in the problem, it is evident that the turbulent diffusivity is proportional to the square root of the jet momentum, and hence is a constant.

It is possible to find a similarity solution for the turbulent jet, or more properly for a point momentum source. To carry this out, it proves convenient to introduce a modified radial dimension

$$\eta = \sqrt{\frac{3}{8}}\,\frac{\sqrt{\mu}}{D}\,\frac{r}{z} \tag{8}$$

where μ is the constant jet momentum flux

$$\mu = \int_0^\infty W^2\, r dr \tag{9}$$

The stream function ψ, with the usual properties that $U = -\frac{1}{r}\frac{\partial \psi}{\partial z}$, $W = \frac{1}{r}\frac{\partial \psi}{\partial r}$, may then be written in the form

$$\psi = D z\, F(\eta) \tag{10}$$

Substitution into the momentum equation, Equation 6, yields the ordinary differential equation for $F(\eta)$

$$-\left\{\frac{1}{\eta} FF'' + \frac{1}{\eta} F'F' - \frac{1}{\eta^2} FF'\right\} = \frac{d}{d\eta}\left(F'' - \frac{1}{\eta} F'\right)$$

which may be integrated once to give

$$-\frac{1}{\eta} FF' = F'' - \frac{1}{\eta} F' \tag{11}$$

the constant of integration being zero because $\frac{1}{\eta} F'$ and F'' vanish for large η. Fortunately, the solution for Equation 11 may be written simply as

$$F(\eta) = \frac{\eta^2}{1 + \frac{1}{4}\eta^2} \tag{12}$$

which satisfies the requirement that the stream function vanish on the symmetry axis, $\eta = 0$, and satisfies identically the momentum conservation relation $\mu = \int_0^\infty W^2 \, r dr$, as

$$\frac{3}{8} \int_0^\infty \left(\frac{F'}{\eta}\right)^2 \eta \, d\eta = 1 \tag{13}$$

The velocity components of the mean flowfield are then

$$W = \frac{3}{8} \frac{\mu}{D} \frac{1}{z}\left(\frac{F'}{\eta}\right)$$

$$= \frac{3}{4} \frac{\mu}{D} \frac{1}{z(1 + \frac{1}{4}\eta^2)^2} \tag{14}$$

and

$$U = - \sqrt{\frac{3}{8}\mu} \frac{1}{z}\left(\frac{F}{\eta} - F'\right)$$

$$= \sqrt{\frac{3}{8}\mu} \frac{1}{z} \frac{\eta(1 - \frac{1}{4}\eta^2)}{(1 + \frac{1}{4}\eta^2)^2} \tag{15}$$

Now explicit solution of the flame density and reactant conservation relations require a quantitative form for the reactant consumption rates. If the chemistry were actually of infinitely fast rate and if the mutual reactants were uncontaminated by products of combustion, the values of $\kappa_1^* v_1$ and $\kappa_2^* v_2^*$ appearing in Equations 3 and 4 could be written

$$\kappa_1^* v_1 = \beta_1 \sqrt{D\varepsilon} \quad ; \quad \kappa_2^* v_2 = \beta_2 \sqrt{D\varepsilon} \tag{16}$$

where D is the coefficient of molecular diffusion, $\varepsilon \equiv \alpha\left|\frac{\partial W}{\partial r}\right|$ is proportional to the turbulent strain rate, and β_1, β_2 are constants for a given chemical

combination, depending upon the reaction stoichiometry. Numerical calculations of strained laminar diffusion flames, which will be discussed later, suggest that for a wide range of flame straining rates and reactant dilutions, the values of $\kappa_1 v_1$ and $\kappa_2 v_2$ may be written

$$\kappa_1 {}^* v_1 = \beta_1 \, G_1(\kappa_1,\kappa_2) \, \sqrt{D\varepsilon} \quad ; \quad \kappa_2 {}^* v_2 = \beta_2 \, G_2(\kappa_1,\kappa_2) \, \sqrt{D\varepsilon} \tag{17}$$

where $G_1(\kappa_1,\kappa_2)$, $G_2(\kappa_1,\kappa_2)$ depend only upon the local average reactant mass fractions and $G_1 = G_2 = 1$ for fast chemistry. The equations for reactant consumption and flame density may then be written

$$U \frac{\partial \kappa_1}{\partial r} + W \frac{\partial \kappa_1}{\partial z} = \frac{1}{r} \frac{\partial}{\partial r} \left(r \, \mathbf{D} \frac{\partial \kappa_1}{\partial r} \right) - \beta_1 \, G_1(\kappa_1,\kappa_2) \, \sqrt{\varepsilon D} \, \Sigma \tag{18}$$

$$U \frac{\partial \kappa_2}{\partial r} + W \frac{\partial \kappa_2}{\partial z} = \frac{1}{r} \frac{\partial}{\partial r} \left(r \, \mathbf{D} \frac{\partial \kappa_2}{\partial r} \right) - \beta_2 \, G_2(\kappa_1,\kappa_2) \, \sqrt{\varepsilon D} \, \Sigma \tag{19}$$

$$U \frac{\partial \Sigma}{\partial r} + W \frac{\partial \Sigma}{\partial z} = \frac{1}{r} \frac{\partial}{\partial r} \left(r \, \mathbf{D} \frac{\partial \Sigma}{\partial r} \right) + \varepsilon \, \Sigma - \lambda \, \beta_1 \, G_1 \frac{\sqrt{D\varepsilon}}{\kappa_1} \Sigma^2 - \lambda \, \beta_2 \, G_2 \frac{\sqrt{D\varepsilon}}{\kappa_2} \Sigma^2 \tag{20}$$

$$\kappa_1 + \kappa_2 + \kappa_3 = 1 \tag{21}$$

When the chemistry is fast, so that $G_1 = G_2 = 1$, it is convenient to use a linear combination of κ_1 and κ_3 that satisfies a homogeneous diffusion equation. Such a combination is $\kappa_1 + \frac{1}{1 + \beta_2/\beta_1} \kappa_3 \equiv J$, and because a diffusion flame with fast chemistry utilizes fuel and oxidizer in the stoichiometric ratio ϕ, the quantity $\beta_2/\beta_1 = \phi$ and

$$J = \kappa_1 + \frac{1}{1+\phi} \kappa_3 \tag{22}$$

Thus $J(r,z)$ satisfies

$$U \frac{\partial J}{\partial r} + W \frac{\partial J}{\partial z} = \frac{1}{r} \frac{\partial}{\partial r} \left(r \, \mathbf{D} \frac{\partial J}{\partial r} \right) \tag{23}$$

with the conditions $J(\infty,z) = 0$ and hence, comparing Equations 23, 6, and 7, it is clear that $J(r,z) \sim W(r,z)$. The constant of proportionality between J and W is easily found by noting that if the actual flow of fuel injected into the stream is γ, then the flow of the product formed is $(1 + \phi)\gamma$ for large values of z where the reaction is complete and $\kappa_1 = 0$. Then the integrated flux of the product is, as $z \to \infty$

$$\int_0^\infty \kappa_3 \, W \, r dr = \gamma(1 + \phi) \tag{24}$$

and because integration of Equation 23 shows that $\int_0^\infty J \, W \, r dr$ is conserved along the z direction, it follows that

$$\int_0^\infty J \, W \, r dr = \gamma \tag{25}$$

Because J is proportional to W, the integral is the same as that evaluated to ensure conservation of momentum with z and hence it follows, comparing Equations 9 and 25, that

$$J = \frac{\gamma}{\mu} W = \frac{3}{8} \frac{\gamma}{D} \frac{1}{z}\left(\frac{F'}{\eta}\right) \tag{26}$$

We have then the algebraic relation

$$\kappa_1 + \frac{1}{1+\phi} \kappa_3 = \frac{3}{8} \frac{\gamma}{D} \frac{1}{z}\left(\frac{F'}{\eta}\right) \tag{27}$$

in addition to the relation Equation 21 and, as a consequence, we need only work with a single species conservation Equation 19.

In order to make this identification between $J(r,z)$ and $W(r,z)$, it has been necessary to introduce the volume flow rate γ as well as the momentum μ of the jet. These two quantities may be used to characterize the jet velocity

$$\text{velocity} \sim \mu/\gamma \tag{28}$$

and the characteristic dimension of the jet,

$$\text{length} \sim \gamma/\sqrt{\mu} \tag{29}$$

when, in fact, the length $\gamma/\sqrt{\mu} = \sqrt{\pi}\, R$, where R is the initial radius of a jet with uniform velocity.

VI. FUEL JET WITH FAST CHEMISTRY

When the chemical reaction rates are fast, the relevant equations, Equations 18, 27, and 20 are simplified principally by the fact that the functions G_1, G_2 are both unity and, in general, $\beta_2 = \phi\ \beta_1$. Now if there were no reactions and if the flame straining were neglibible ($\varepsilon = 0$), then the problem would possess similarity solutions of the form $\kappa_1 \sim \frac{1}{z} k_1(\eta)$ and $\Sigma \sim \frac{1}{z} \sigma(\eta)$. There is a certain advantage in writing these quantities in that form, as

$$\kappa_1 = \frac{3}{8} \frac{\gamma}{D} \frac{1}{z} k_1(\eta,z) \tag{30}$$

and

$$\Sigma = \frac{3}{8} \left(\frac{\sqrt{\mu}}{\alpha D}\right)^{1/2} \frac{1}{\beta_1 z} \sigma(\eta,z) \tag{31}$$

Now because we shall use an integral technique to obtain our final result, it is convenient to rewrite Equations 18 and 20 in similarity variables and integrate them over the flame cross section. Introducing the similarity coordinates, η and z, we have

$$\frac{\sqrt{\frac{3}{8}\mu}}{D} \frac{1}{z} \frac{\partial}{\partial \eta} (r\ U\ \kappa_1) + \frac{\partial}{\partial z} (r\ W\ \kappa_1) - \frac{1}{z} \frac{\partial}{\partial \eta} (\eta\ r\ W\ \kappa_1) + \frac{r}{z} W\ \kappa_1$$

$$= \frac{\sqrt{\frac{3}{8}\mu}}{D} \frac{1}{z} \frac{\partial}{\partial \eta} \left(r\ D \frac{\partial \kappa_1}{\partial r}\right) - \beta_1 \sqrt{\alpha D \left|\frac{\partial W}{\partial r}\right|}\ r\ \Sigma \tag{32}$$

and

$$\frac{\sqrt{\frac{3}{8}\mu}}{D} \frac{1}{z} \frac{\partial}{\partial \eta} (r\ u\ \Sigma) + \frac{\partial}{\partial z} (r\ W\ \Sigma) - \frac{1}{z} \frac{\partial}{\partial \eta} (\eta\ r\ W\ \Sigma) + \frac{1}{z} (r\ W\ \Sigma)$$

$$= \frac{\sqrt{\frac{3}{8}\mu}}{D} \frac{1}{z} \frac{\partial}{\partial \eta} \left(r\ D \frac{\partial \Sigma}{\partial r}\right) + \alpha \left|\frac{\partial W}{\partial r}\right|\ r\ \Sigma - \lambda \sqrt{\alpha D \left|\frac{\partial W}{\partial r}\right|}\ \beta_1\ r\ \Sigma \frac{\Sigma}{\kappa_1 \kappa_2} \tag{33}$$

Integrate these from $\eta = 0$ to $\eta = \infty$ and take account of the behavior of κ_1 and Σ for large radii. We then have from Equation 32

$$\frac{d}{d\xi}\int_0^\infty \left(\frac{F'}{\eta}\right) k_1\,(\eta,\xi)\,\eta\,d\eta = -\left(\frac{3}{8}\right)^{3/4}\int_0^\infty \sqrt{\frac{d}{d\eta}\left(-\frac{F'}{\eta}\right)}\;\sigma(\eta,\xi)\,\eta\,d\eta \tag{34}$$

where we have introduced a new variable for distance along the axis,

$$\xi = \frac{8}{3}\frac{D}{\gamma}\,z \tag{35}$$

Treating the flame density relation in the same manner

$$\frac{d}{d\xi}\int_0^\infty \left(\frac{F'}{\eta}\right)\sigma\;\eta(\xi,\eta)\;d\eta = \left(\frac{3}{8}\right)^{1/2}\frac{\alpha\sqrt{u}}{D}\int_0^\infty \frac{d}{d\eta}\left(-\frac{F'}{\eta}\right)\sigma(\eta,\xi)\eta\;d\eta$$

$$-\lambda\left(\frac{3}{8}\right)^{3/4}\int_0^\infty \sqrt{\frac{d}{d\eta}\left(-\frac{F'}{\eta}\right)}\frac{\sigma^2(\eta,\xi)}{k_1\,\kappa_2}\,\eta\,d\eta \tag{36}$$

where in this notation

$$\kappa_2 = 1 - \frac{1}{\xi}\left((1+\phi)\,\frac{F'}{\eta} - \phi\,k_1\right) \tag{37}$$

To complete the solution using the integral technique, it is required to select profile shapes for the mass fraction distribution and for the flame surface density. These are chosen specifically in the following form:

$$k_1(\eta,\xi) = \left(\frac{F'}{\eta}\right)\left(1 - f(\xi)\right) \tag{38}$$

$$\kappa_2(\eta,\xi) = 1 - \left(\frac{F'}{\eta}\right)\frac{1}{\xi}\left(1 + \phi\,f(\xi)\right) \tag{39}$$

$$\sigma(\eta,\xi) = \left(\frac{F'}{\eta}\right) h(\xi) \left(1 - f(\xi)\right) \left[1 - \left(\frac{F'}{\eta}\right) \frac{1}{\xi} \left(1 + \phi\, f(\xi)\right)\right] \tag{40}$$

where $f(\xi)$ and $h(\xi)$ are unknown functions of distance along the axis and will be determined through the integral relations, Equations 34 and 36. Without justifying this choice in detail, several properties are important:

a) They are exact when there is no chemical reaction.

b) They satisfy exactly the conditions given by Equation 27 among species mass fractions.

c) They satisfy the appropriate boundary conditions at the symmetry axis and at distances remote from the axis.

d) The flame surface density vanishes, as it must physically, where either the fuel or oxidizer reactants vanish.

Now the value of $F(\eta) = \eta^2/(1 + \frac{1}{4}\eta^2)$, Equation 12, is the exact solution for the stream function in the jet problem utilizing the turbulent diffusivity formulation. Utilizing this and the representations for $k_1(\eta,\xi)$, $\kappa_2(\eta,\xi)$, $\sigma(\eta,\xi)$ given in Equations 38, 39, and 40, the integrations indicated in the integral relations, Equations 34 and 36, may be carried out. The integrals are of three classes: (i) those which may be carried out in an elementary manner, (ii) those which may be reduced to an integral of $(1 + \frac{1}{4}\ ^2)^{-n}$ and have the value

$$\int_0^\infty \frac{d\eta}{\left(1 + \frac{1}{4}\eta^2\right)^n} = \pi \prod_{j=1}^{n-1} \left(\frac{2(n-j) - 1}{2(n-j)}\right) \tag{41}$$

and (iii) those of the form

$$I_n = \int_0^\infty \left(\frac{F'}{\eta}\right)^n F' \sqrt{\frac{2\eta}{\left(1 + \frac{1}{4}\eta^2\right)^3}}\, d\eta \tag{42}$$

These may, after a transformation, be written as

$$I_n = (2)^{n+3}\, B\left(2n + 2 + \frac{1}{4} \;;\; 5/4\right) \tag{43}$$

$$= (2)^{n+3}\, \frac{\Gamma\left(2n + 2 + \frac{1}{4}\right)\Gamma(5/4)}{\Gamma\left(2n + 3 + \frac{1}{2}\right)} \tag{44}$$

where both the Beta function and Gamma function representations are tabulated.

If we carry out this somewhat lengthy task on Equations 34 and 36, a pair of non-linear ordinary differential equations results

$$\frac{d}{d\xi}(1-f) = -\left\{0.44424 - 0.41251\left(\frac{1 + \phi f}{\xi}\right)\right\}(1-f)h \tag{45}$$

$$\frac{d}{d\xi}\left\{\left[1 - \frac{6}{5}\left(\frac{1 + \phi f}{\xi}\right)\right](1-f)h\right\} = \frac{\alpha\sqrt{\mu}}{D}\left[0.45090 - 0.47344\left(\frac{1 + \phi f}{\xi}\right)\right]\frac{(1-f)h}{\xi}$$

$$- \lambda\,(1-f)h^2\,(0.25386)\left[1 - \frac{13}{14}\left(\frac{1 + \phi f}{\xi}\right)\right] \tag{46}$$

These are to be integrated from $\xi_0 \tilde{=} 2$, the virtual origin of the jet being at $\xi = 0$, to an arbitrary value of ξ; the initial values of $f(\xi_0) = 0$ and $h(\xi_0) \equiv h_0$, where h_0 gives a measure of the amount of flame surface that is present at the start of calculation. Physically, the initial value of $h(\xi_0)$ is related to an ignition process which the turbulent flame model does not, of course, describe. It is to be expected that varying the initial value h_0 will have a significant effect upon the local structure of the flame, but a much smaller effect upon the development far from the origin. The values of ϕ and $\frac{\sqrt{\mu}}{D}$ are fixed by the reactants and by the turbulence model, respectively. The values of α and λ, on the other hand, are numerical constants which are universal in the sense that they do not depend upon stoichiometry, momentum flux, or geometrical size of the problem.

VII. THE STRAINED LAMINAR FLAME

This section describes the strained laminar flame calculations which provide the reactant consumption and nitric oxide production rates used in the model. When the chemical rates are taken to be infinitely fast, an analytical solution yields the fuel and oxidizer rates written in Equation 16 and applied in Section IV:

$$\kappa_1^* v_1 = \beta_1 \sqrt{D\varepsilon} \quad ; \quad \kappa_2^* v_2 = \beta_2 \sqrt{D\varepsilon} \tag{47}$$

In the more general case in which fluid properties are variable, heats of reaction and kinetic rates are finite, and many chemical reactions are treated, a numerical calculation is required. The results presented in this section come from such a calculation and are the work of T. J. Tyson and his associates at the Energy and Environmental Research Corporation. The authors acknowledge with thanks their cooperation in making the results available and thank especially C. J. Kau who made, under difficult circumstances, the many computer runs we requested. The set of kinetic equations describing the methane-air reactions in the computer program were developed by the Energy and Environmental Research Corporation staff under Environmental Protection Agency Contract Number 68-02-2631 and were reported in their Monthly Progress Report No. 14, June 1978.

For the reasons given in Section III, solutions are needed for a range of strain rates and for various dilutions of the fuel and oxidizer by combustion products. The thermodynamic states of the diluted reactants are those reached when products in the form of CO_2, H_2O, and N_2 are added adiabatically to the reactants and no chemical reaction is allowed.

The combination of strain rates and dilution ratios for which calculations were made and the results are given in Table 1. (Several cases were omitted initially due to the lack of time, but were determined to be not needed when the results were examined.)

Table 1. STRAINED FLAME METHANE-AIR REACTION RATES

CASE	% AIR	% FUEL	STRAIN RATE, SEC^{-1}	REACTION RATE, MOLES/CM^2-SEC			$\beta_1 G_1$	$\frac{1}{2} \beta_2 G_2$
				CH_4	O_2	NO		
1	1.0	1.0	50	$2.9 \cdot 10^{-5}$	$4.75 \cdot 10^{-5}$	$3.5 \cdot 10^{-9}$	0.142	0.232
			250	6.68	10.4	1.04	0.146	0.228
			500	9.22	13.6	0.42	0.143	0.210
2	1.0	0.75	50	2.32	3.89	4.19	0.114	0.19
			200	4.60	7.56	1.56	0.113	0.185
3	1.0	0.50	50	1.96	3.3	5.99	0.096	0.161
			200	3.98	6.45	2.47	0.097	0.158
			400	6.0	9.07	1.28	0.104	0.157
			600	7.43	10.9	0.94	0.105	0.154
4	1.0	0.25	50	1.57	2.65	9.3	0.077	0.130
			200	3.24	5.23	3.98	0.079	0.128
			400	4.74	7.32	2.63	0.082	0.127
			600	5.89	8.90	1.91	0.083	0.126
6	0.75	0.75	50	2.02	3.27	5.57	0.099	0.160
			200	4.78	6.44	2.41	0.105	0.158
			400	6.22	8.96	1.25	0.108	0.155
			600	7.69	10.8	0.77	0.109	0.153
7	0.75	0.50	50	1.71	2.80	7.34	0.084	0.137
			200	3.60	5.51	3.45	0.088	0.135
			400	5.26	7.75	2.01	0.091	0.134
			600	6.53	9.33	1.35	0.092	0.132
8	0.75	0.25	50	1.38	2.26	10.5	0.068	0.111
			200	2.87	4.46	5.17	0.070	0.109
			400	4.18	6.25	3.21	0.072	0.108
			600	5.20	7.58	2.40	0.073	0.107
10	0.50	0.75	50	1.59	2.44	7.14	0.078	0.119
			200	3.39	4.79	3.66	0.083	0.117
			600	6.13	8.0	1.68	0.087	0.113
11	0.50	0.50	50	1.35	2.09	8.69	0.066	0.102
			200	2.86	4.13	4.69	0.070	0.101
			400	4.20	5.78	3.10	0.073	0.100
			600	5.22	6.46	2.31	0.074	0.098
12	0.50	0.25	50	7.11	1.72	11.1	0.054	0.084
			200	2.31	3.41	6.24	0.057	0.083
			400	3.38	4.77	4.31	0.058	0.083
			600	4.21	5.76	3.33	0.059	0.081
14	0.25	0.75	50	1.02	1.4	8.46	0.050	0.069
			200	2.21	2.72	5.19	0.054	0.067
			400	3.25	3.77	3.77	0.056	0.065
			600	3.99	4.45	2.94	0.056	0.063
15	0.25	0.50	50	0.88	1.21	9.52	0.043	0.059
			200	1.88	2.37	5.95	0.046	0.058
			400	2.77	3.30	4.43	0.048	0.057
			600	3.44	3.94	3.58	0.049	0.054
16	0.25	0.25	50	0.75	1.02	11.2	0.037	0.050
			200	1.55	2.01	6.93	0.038	0.049
			400	2.27	2.80	5.25	0.039	0.048
			600	2.83	2.35	4.35	0.040	0.047

In Section III, Equation 17, the fuel and oxidizer comsumption rates were written in the form:

$$\kappa_1^* v_1 = \beta_1 G_1(\kappa_1,\kappa_2) \sqrt{D\varepsilon} \quad ; \quad \kappa_2^* v_2 = \beta_2 G_2(\kappa_1,\kappa_2) \sqrt{D\varepsilon} \tag{48}$$

The functions $\beta_1 G_1$ and $\beta_2 G_2$ are also given in Table 1 and, for each composition, are indeed almost independent of the strain as they are, exactly, when the reaction rates are infinite. The average values of these functions for each dilution ratio are collected in Table 2. Only the function for the fuel is needed and is represented with acceptable accuracy by the expressions:

$$\beta_1 = 0.142 \tag{49}$$

$$G_1 = \frac{3}{7}\kappa_1 + \frac{4}{7}\kappa_2 \tag{50}$$

The treatment of the nitric oxide production rate is somewhat more empirical. It was noted that this rate decreased approximately with $\varepsilon^{-1/2}$. We introduce, therefore, the variable H/τ defined by

$$\frac{H}{\tau} = \frac{\dot{\omega}_{NO}\, \varepsilon^{1/2}}{\rho \sqrt{D}} , \tag{51}$$

where $\dot{\omega}_{NO}$ is NO production in mass per unit flame area per unit time, and observe that the dependence of the NO production on strain is represented within about a factor of two in this way. The values of H/τ for cases 3 and 12, shown in Table 3, are representative examples. Average values for all compositions are given in Table 4 and were found to depend, approximately, linearly upon the variable $(\kappa_1 + \kappa_2)$, as Figure 1 shows. The fit to this data used in the analysis in Section VI is

$$\frac{1}{\tau} = 4 \times 10^{-3}\ \text{sec}^{-1} \tag{52}$$

$$H = \{2 - (\kappa_1 + \kappa_2)\} \tag{53}$$

Table 2. FUEL AND OXIDIZER CONSUMPTION FUNCTIONS

β_1 G_1				
κ_2 \ κ_1	1	0.75	0.50	0.25
1.00	0.142	0.113	0.100	0.080
0.75	0.123	0.105	0.088	0.070
0.50	0.098	0.084	0.046	0.038
0.25	0.060	0.053	0.046	0.038
β_2 G_2				
κ_2 \ κ_1	1	0.75	0.50	0.25
1.00	0.44	0.38	0.31	0.256
0.75	0.376	0.314	0.268	0.218
0.50	0.246	0.232	0.20	0.166
0.25	0.150	0.132	0.114	0.096

Table 3. NITRIC OXIDE PRODUCTION FUNCTION; DEPENDENCE ON STRAIN RATE

Case	ε	$H/\tau \times 10^3$
3	50	27.5
	200	22.7
	400	16.6
	600	14.9
12	50	50.9
	200	57.3
	400	55.9
	600	52.9

Table 4. NITRIC OXIDE PRODUCTION FUNCTION

Case	$H/\tau \times 10^3$	Case	$H/\tau \times 10^3$
1	1.0	10	3.0
2	1.4	11	4.2
3	2.0	12	5.6
4	3.5	14	4.8
6	2.0	15	5.6
7	2.9	16	6.6
8	4.5		

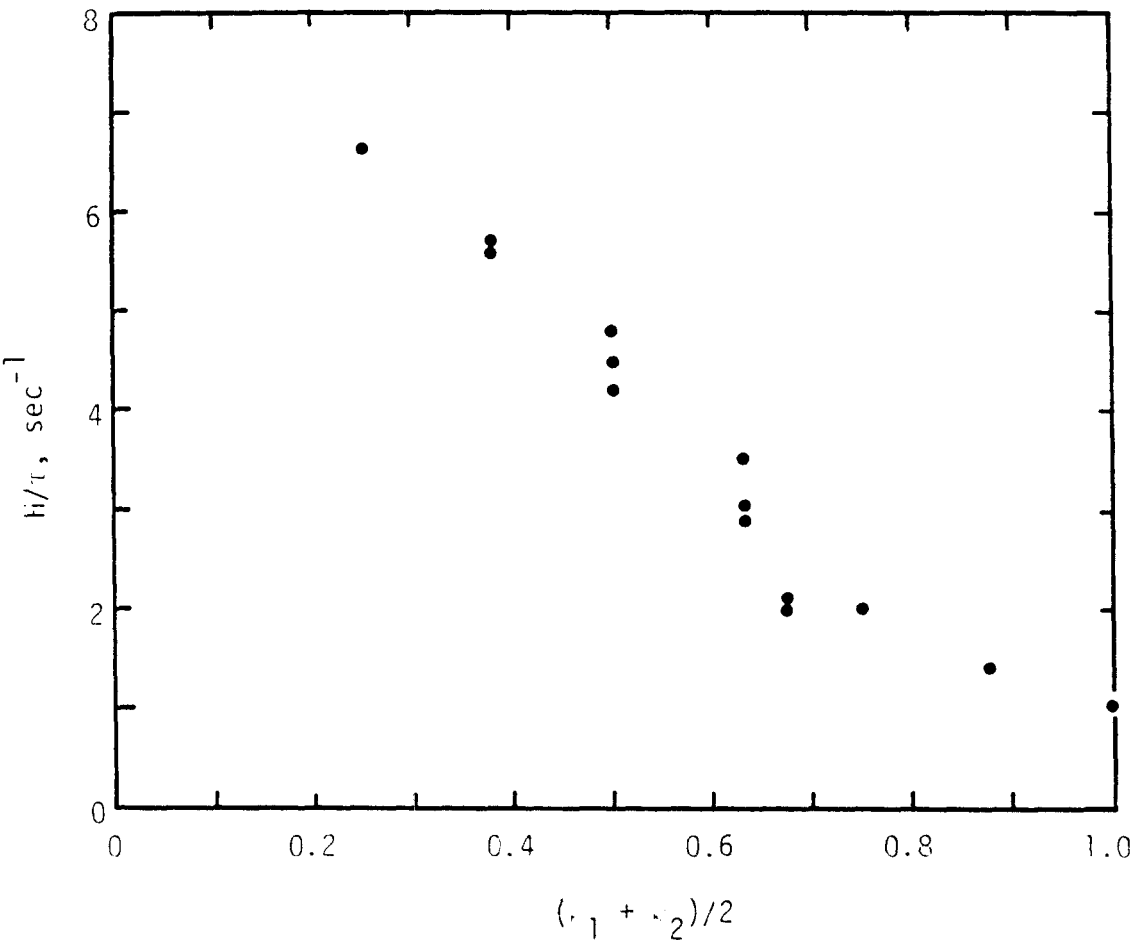

Figure 2. Dependence of nitric oxide production on reactant dilution

It is significant that the chemical kinetics code from which these calculations were made, gives the result, shown in Figure 2, that NO production rate actually increases as the reactants are diluted with hot combustion products. This result might not have been expected, but because examination of this code was not the aim of the present work, this interesting result was not examined in detail. One may speculate that the increase of flame temperature accompanying reactant dilution and the "re-processing" of combustion product in the hot flame contribute to this trend.

The computations which yield the above discussed rates also determine the detailed structure of the laminar flame. A complete set of concentration profiles and the temperature distribution for case 6 are shown in Figures B-1 through B-8 in Appendix B. Figures B-9 through B-11 contain a few results for the same reactant compositions, but a lower strain rate. Since a

thorough examination of these results remains to be done, no further analysis will be presented at this time.

VIII. NITRIC OXIDE PRODUCTION IN FUEL JET

If we denote by κ_N the mass fraction of nitric oxide, we may write the nitric oxide conservation (or production) relation as

$$U \frac{\partial \kappa_N}{\partial r} + W \frac{\partial \kappa_N}{\partial z} = \frac{1}{r} \frac{\partial}{\partial r} \left(r D \frac{\partial \kappa_N}{\partial r} \right) + \frac{1}{\tau} H(\kappa_1, \kappa_2) \sqrt{\frac{D}{\varepsilon}} \Sigma \tag{54}$$

where the rate relation for the production of nitric oxide, developed in the preceding section, has been employed. In this expression, $1/\tau$ is an absolute rate constant, and $H(\kappa_1, \kappa_2)$ is the function that accounts for the effects of free stream reactant dilution upon nitric oxide production within the flame. If Equation 54 is rewritten in the form

$$\frac{\partial}{\partial r} \left(r U \kappa_N \right) + \frac{\partial}{\partial z} \left(r W \kappa_N \right) = \frac{\partial}{\partial r} \left(r D \frac{\partial \kappa_N}{\partial r} \right) + \frac{1}{\tau} H(\kappa_1, \kappa_2) \sqrt{\frac{D}{\varepsilon}} r \Sigma \tag{55}$$

use of the similarity variables and the stream function leads to the result

$$\begin{aligned} &- \frac{\partial}{\partial \eta} \left\{ \frac{\eta}{z} \left(\frac{F}{\eta} - F' \right) \kappa_N \right\} + \frac{\partial}{\partial z} \left\{ \eta \left(\frac{F'}{\eta} \right) \kappa_N \right\} - \frac{1}{z} \frac{\partial}{\partial \eta} \left\{ \eta^2 \left(\frac{F'}{\eta} \right) \kappa_N \right\} \\ &\quad + \frac{1}{z} \left(\eta \left(\frac{F'}{\eta} \right) \kappa_N \right) = \frac{\partial}{\partial \eta} \left\{ \eta \frac{\partial \kappa_N}{\eta} \right\} \\ &\quad + \frac{8}{3} \frac{zD}{\mu} \ell H(\kappa_1, \kappa_2) \eta \sqrt{\frac{D D^2 z^2}{\left(\frac{3}{8} \mu \right)^{3/2}} / \frac{d}{d\eta} \left(- \frac{F'}{\eta} \right)} \Sigma \end{aligned} \tag{56}$$

where we define $\ell = 1/\tau\sqrt{\alpha}$.

Now we wish to calculate the ratio of nitric oxide flux $\int_0^\infty \rho W \kappa_N (2\pi r) dr$ to the total product flux $\int_0^\infty \rho W (2\pi r) dr$ and this ratio becomes

$$\int_0^\infty \rho\, W\, \kappa_N\, (2\pi r)\, dr \Big/ \int_0^\infty \rho\, W\, (2\pi r)\, dr = \int_0^\infty \kappa_N \left(\frac{F'}{\eta}\right)\eta\, d\eta \Big/ \int_0^\infty \left(\frac{F'}{\eta}\right)\eta\, d\eta$$

But the integral in the denominator is equal to 4/3 and, hence,

$$\Phi_N = \frac{3}{4}\int_0^\infty \kappa_N \left(\frac{F'}{\eta}\right)\eta\, d\eta \tag{57}$$

Thus if, returning to Equation 56, we integrate this over the jet cross section and take account of behavior of the stream function at large radii

$$\left\{\frac{d}{dz} + \frac{1}{z}\right\}\int_0^\infty \kappa_N \left(\frac{F'}{\eta}\right)\eta\, d\eta$$

$$= \left(\frac{8}{3}\right)^{3/2} \frac{\ell\, z^2\, D^2}{\mu \sqrt{\frac{3}{8}}^{1/2}\, \mu} \sqrt{\frac{D}{\mu^{1/2}}} \int_0^\infty \left[\frac{d}{d\eta}\left(-\frac{F'}{\eta}\right)\right]^{-1/2} H\, \Sigma\, \eta\, d\eta$$

or

$$\left\{\frac{d}{dz} + \frac{1}{z}\right\}\Phi_N = 2\left(\frac{8}{3}\right)^{3/4} \frac{\ell\, D^2}{\mu^{3/2}} \sqrt{\frac{D}{\mu^{1/2}}}\, z^2 \int_0^\infty \left[\frac{d}{d\eta}\left(-\frac{F'}{\eta}\right)\right]^{-1/2} H\, \Sigma\, \eta\, d\eta \tag{58}$$

Now this expression may be put in a more suitable form for integration by introducing the dimensionless distance along the axis, ξ, Equation 35, and the representation of the flame surface area, Σ, given by Equation 31. The resulting relation

$$\left(\frac{d}{d\xi} + \frac{1}{\xi}\right)\Phi_N = 2\left(\frac{3}{8}\right)^{9/4} \frac{\ell}{\beta_1}\left(\frac{\gamma^2}{\mu^{3/2}}\right)\xi \int_0^\infty H\, \sigma \left\{\frac{d}{d\eta}\left(-\frac{F'}{\eta}\right)\right\}^{-1/2} \eta\, d\eta \tag{59}$$

contains a dimensionless group $(\ell/\beta_1)\ (\gamma^2/\mu^{3/2})$ which will be of considerable physical significance in developing the scaling laws for the production of nitric oxide in flame structures. The volume flow, γ, and momentum flow, μ,

may be represented in the forms

$$\mu = W_0^2 \left(\frac{R^2}{2}\right)$$

$$\gamma = W_0 \left(\frac{R^2}{2}\right)$$

where W_0 is the effective average velocity from a jet of radius R. Substitution of these expressions into Equation 59 yields the equation for the nitric oxide concentration

$$\left(\frac{d}{d\xi} + \frac{1}{\xi}\right) \Phi_N = \frac{\ell}{\beta_1} \frac{d}{W_0} \left(2^{-1/2}\right)\left(\frac{3}{8}\right)^{9/4} \int_0^\infty \xi \left\{\frac{d}{d\eta}\left(-\frac{F'}{\eta}\right)\right\}^{-1/2} H \sigma \eta \, d\eta \qquad (60)$$

where $d = 2R$ is the initial jet diameter.

The representation of $\sigma(\eta,\xi)$, appropriate to the integral solution, is given by Equation 40, and the function $H(\kappa_1,\kappa_2)$, developed in the preceding section, will be written

$$\begin{aligned} H(\kappa_1,\kappa_2) &= 2 - (\kappa_1 + \kappa_2) \\ &= 1 + \kappa_3 \\ &= 1 + (1 + \phi)\frac{f}{\xi}\left(\frac{F'}{\eta}\right) \end{aligned} \qquad (61)$$

These relations for $\sigma(\eta,\xi)$ and $H(\kappa_1,\kappa_2)$ allow the integration to be carried out in the following manner. Writing the integral in detail

$$\begin{aligned} \int_0^\infty \xi \left\{\frac{d}{d\eta}\left(-\frac{F'}{\eta}\right)\right\}^{-1/2} H \sigma \eta \, d\eta &= \xi(1-f)h \int_0^\infty \left\{\frac{d}{d\eta}\left(-\frac{F'}{\eta}\right)\right\}^{-1/2} \left(\frac{F'}{\eta}\right)^2 \eta \, d\eta \\ &+ (1-f)h\,\phi(1-f) \int_0^\infty \left\{\frac{d}{d\eta}\left(-\frac{F'}{\eta}\right)\right\}^{-1/2} \left(\frac{F'}{\eta}\right)^3 \eta \, d\eta \\ &- (1-f)h\,(1+\phi f)(1+\phi)\frac{f}{\xi} \int_0^\infty \left\{\frac{d}{d\eta}\left(-\frac{F'}{\eta}\right)\right\}^{-1/2} \left(\frac{F'}{\eta}\right)^4 \eta \, d\eta \end{aligned} \qquad (62)$$

In a manner similar to the procedure used in evaluating certain of the integrals in the flame surface density earlier, each of these integrals is of the form

$$\int_0^\infty \left\{\frac{d}{d\eta}\left(-\frac{F'}{\eta}\right)\right\}^{-1/2} \left(\frac{F'}{\eta}\right)^n \eta \, d\eta \equiv J_n \tag{63}$$

where we know $F(\eta)$ so that

$$\frac{F'}{\eta} = 2\left(1 + \frac{1}{4}\eta^2\right)^{-2}$$

With some variable transformation and rearrangement, we may find that

$$\begin{aligned} J_n &= 2^n B\left\{2(n-1) - \frac{1}{4} \; ; \; \frac{3}{4}\right\} \\ &= 2^n \frac{\Gamma\left\{2(n-1) - \frac{1}{4}\right\} \Gamma\left\{\frac{3}{4}\right\}}{\Gamma\left(2n - \frac{3}{2}\right)} \end{aligned} \tag{64}$$

and, thus, the integrals may be evaluated numerically with the aid of tabulated values of the real gamma function.

If these numerical evaluations are carried out and we define a variable P_N, proportional to the nitric oxide formation,

$$\Phi_N = \left(\frac{1}{\beta_1}\right)\left(\frac{k\,d}{W_0}\right) P_N \tag{65}$$

The differential equation for P_N is then

$$\begin{aligned} \frac{d\,P_N}{d\xi} = &- \frac{1}{\xi} P_N + \left\{0.058308\,\xi + 0.063842\,\phi\,(1 - f)\right. \\ &\left. - 0.091893\,(1 + \phi)\,\frac{f(1 + \phi\,f)}{\xi}\right\}(1 - f)h \end{aligned} \tag{66}$$

which is to be solved in conjunction with Equations 45 and 46 for the reacting jet structure.

IX. FUEL JET WITH FINITE RATE CHEMISTRY

The calculations for the detailed structure of methane flames, discussed in Section V, permit a somewhat more realistic description of the turbulent flame structure than that afforded by the fast chemistry employed in Section IV. In addition, because these calculations were carried out with various degrees of reactant dilution with combustion products, it is possible to account for the dilution of the unburned reactants which takes place as one proceeds along the jet. It will be recalled that the model described in Section IV, the combustion rate was entirely diffusion controlled and the reactant concentration far from the flame structure is assumed to be that of the uncontaminated reactants supplied to the jet and the oxidizer field. This is certainly a limit, in one sense, because the consumption per unit area of the flame is a maximum and, hence, the total flame surface area required to consume the fuel in the jet, is a minimum. It is reasonably evident, then, that the nitric oxide produced within the flame itself is well below the actual physical value, if not a minimum.

Another sort of limit that may now be considered follows from the assumption that the combustion products, which are produced in burned out portions of flame, are immediately mixed with the reactants. In this limit, the values of κ_1, κ_2 with which to evaluate the laminar flame structure are the local mean values which we employ in our flame model.

The fact that extensive numerical calculations of Section V show that the reactant consumption rate per unit area is proportional to $\sqrt{D\varepsilon}$ permits the representation for fast chemistry to be carried over not only for finite reaction rates but also for contaminated reactants. Referring again to Equation 17, we select

$$\beta_1 = 0.142 \tag{67}$$

$$G_1(\kappa_1,\kappa_2) = \frac{3}{7}\kappa_1 + \frac{4}{7}\kappa_2 \tag{68}$$

on the basis of the calculations described in Section V. Thus, omitting the details of a calculation which parallels quite closely that of Section IV, the integrated fuel consumption and flame surface density equations are

$$\frac{d}{d\xi}\int_0^\infty \left(\frac{F'}{\eta}\right) k_1(\eta)\eta \, d\eta$$

$$= -\left(\frac{3}{8}\right)^{3/4} \int_0^\infty \left\{\frac{d}{d\eta}\left(-\frac{F'}{\eta}\right)\right\}^{1/2} \left(\frac{3}{7}\kappa_1 + \frac{4}{7}\kappa_2\right) \sigma(\eta,\xi)\eta \, d\eta \qquad (69)$$

and

$$\frac{d}{d\xi}\int_0^\infty \left(\frac{F'}{\eta}\right) \sigma(\eta,\xi)\eta \, d\eta = \left(\frac{3}{8}\right)^{1/2} \left(\frac{\alpha\sqrt{\mu}}{D}\right) \int_0^\infty \frac{d}{d\eta}\left(-\frac{F'}{\eta}\right) \sigma(\eta,\xi)\eta \, d\eta$$

$$- \lambda \left(\frac{3}{8}\right)^{3/4} \int_0^\infty \left\{\frac{d}{d\eta}\left(-\frac{F'}{\eta}\right)\right\}^{1/2} \frac{\sigma^2(\eta,\xi)}{k_1 \kappa_2} \left(\frac{3}{7}\kappa_1 + \frac{4}{7}\kappa_2\right) \eta \, d\eta \qquad (70)$$

which are the counterparts of Equations 34 and 36 that were valid for undiluted reactants. The forms of k_1, κ_2, σ, given by Equations 38, 39, and 40, and the known function $F(\eta)$ allow the explicit evaluation of the integrals that occur utilizing again the results given by Equations 42 through 44 which were useful in developing the equations for the fuel jet and fast chemistry. These relations are then, in detail required for numerical computation,

$$\frac{d}{d\xi}(1-f) = -A\,g \qquad (71)$$

$$C\frac{dg}{d\xi} = \frac{\alpha\sqrt{\mu}}{D} B \frac{g}{\xi} - \lambda A \frac{(g)^2}{1-f} \qquad (72)$$

where a new variable

$$g(\xi) \equiv \left[1 - \frac{6}{5}\left(\frac{1+\phi-f}{\xi}\right)\right](1-f)h \qquad (73)$$

has been introduced. The variable coefficients are

$$A = 0.25386 \frac{1 - \frac{13}{14}\frac{1+\phi f}{\xi}}{1 - \frac{6}{5}\frac{1+\phi f}{\xi}} + 0.17679 \left(\frac{1-f}{\xi} - \frac{4}{3}\frac{1+\phi f}{\xi}\right) \frac{1 + \frac{5}{4}\frac{1+\phi f}{\xi}}{1 - \frac{6}{5}\frac{1+\phi f}{\xi}} \quad (74)$$

$$B = 0.45090 \left(1 - \frac{21}{20}\frac{1+\phi f}{\xi}\right) \quad (75)$$

$$C = 1 - \frac{6}{5}\frac{1+\phi f}{\xi} \quad (76)$$

It will be found, upon detailed inspection, that Equations 71 and 72 reduce to Equations 45 and 46, respectively, when the second term in A, Equation 74, is deleted.

X. RESULTS OF SPECIFIC JET CALCULATIONS

The model of turbulent chemical reactions in fuel jets, which has been presented, rests upon three empirical constants which, if the physics of the model were accurate, would be universal constants. While this universality is not likely, it is to be hoped that the results will be general for turbulent fuel jets and for flows that are reasonably similar to fuel jets. The first of these, which in our representation appears as $\sqrt{\mu}/\mathbf{D}$, is well known and valid for all turbulent jets and, as a matter of fact, does not enter explicitly in our calculations. The second empirical constant is $\alpha\sqrt{\mu}/\mathbf{D}$ which enters in connection with the turbulent straining of the flame surface area. It is well known that the turbulent straining rate in a field of inhomogeneous turbulence is related to the mean flow in a manner that depends upon the type of field (i.e., turbulent jet, mixing region, boundary layer, etc.) but is the same for similar flow fields. Thus, when we assume the turbulent straining of the flame surface to be directly proportional to the straining rate of the mean flowfield, we acknowledge an unknown constant of proportionality, but one that will be of the same value for all turbulent fuel jets. This proportionality appears in the form $\alpha\sqrt{\mu}/\mathbf{D}$.

The flame shortening process is probably the most controversial of the features in the turbulent combustion model which we have presented. If the physical picture, based upon the consumption of regions of fuel or oxidizer, is substantially correct, then there is a constant of proportionality which, for a specific type of turbulent flowfield, connects the actual annihilation of flame surface to the related dimensionless quantities which result from our model. This constant appears as λ in our calculations.

Now even a cursory appraisal of the equation describing the development of the flame surface area suggests that the values of $\alpha\sqrt{\mu}/\mathbf{D}$ and λ are intimately related to the beginning and end of the jet, respectively. When the flame is first ignited, for low values of ξ, the value of $\alpha\sqrt{\mu}/\mathbf{D}$ determines both the rate of growth of flame surface area and the reactant

consumption per unit area. But as the flame density grows and regions within the flame develop where one of the reactant concentration values is low, the terms describing the annihilation of flame surface become important and balance, to some extent, the flame surface growth resulting from turbulent straining. A sort of balance is reached between the straining and annihilation terms, respectively, proportional to $\alpha \sqrt{\mu}/D$ and to λ, which sets the rate at which reactants are consumed in the jet. Together they determine the length of the flame required to consume the fuel. The two quantities also determine the growth of combustion intensity at the beginning of the flame and the point along the flame length at which the combustion intensity reaches its peak.

Because these quantities are readily observable from experiments with gaseous fuel jets, the suitable values for the parameter have been determined in previous work to be approximately

$$\lambda = 5.0$$

$$\frac{\alpha \sqrt{\mu}}{D} = 2.0$$

These values are based largely upon the extensive experiments of Hawthorne, et al.[3] These same data have allowed a satisfactory check of the variations of flame length with fuel stoichiometry.

Using the model described, together with values of the two constants thus determined, calculations have been made for the production of nitric oxide in fuel jets burning methane in air at atmospheric pressure and temperature. The first of these calculations used Equations 45 and 46, describing the fuel jet with fast chemistry and undiluted reactants, together with the differential equation, Equation 66, describing the production of nitric oxide within the flame structure. The interesting result of this computation is shown in Figure 3 where quantities proportional to the centerline fuel concentration and the integrated average nitric oxide

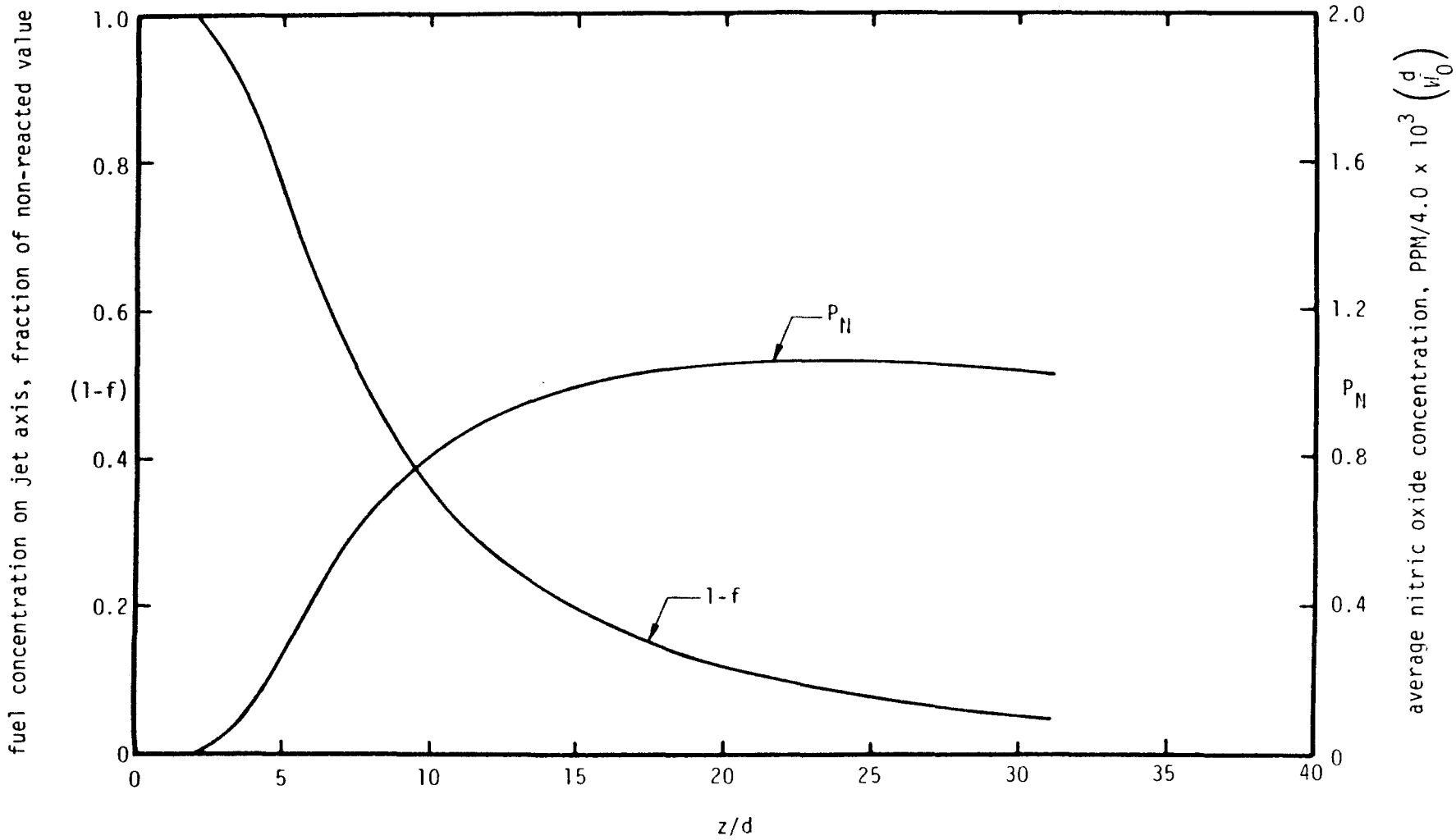

Figure 3. Fuel concentration on jet axis and integrated nitric oxide concentration. Methane-air flame; fast kinetics and no reactant dilution.

concentration are shown as functions of the distance from the virtual origin of the jet measured in terms of the initial jet diameter. The quantity 1-f, referring to Equations 30 and 38, measures the centerline fuel concentration as a fraction of the value that would be observed if there were no chemical consumption of fuel, but only that dilution which would result from mixing with the ambient gas. This, if 1-f remained at the value unity, no chemical reaction would be taking place. Conversely, when 1-f appraoches zero, it signifies that the fuel has been consumed, not simply mixed with a non-reacting diluent, until it is scarely detectable. The nitric oxide concentration P_N, defined by Equation 65, increases very rapidly at the start of flame, levels off, and then drops slightly as the flame end is approached. To interpret this behavior physically, one must recall that the nitric oxide concentration is averaged over the entire jet including all entrained but unburned oxidizer. The initial rise parallels that of the flame surface density because, until the flame annihilation mechanism begins to be important, the nitric oxide is retained within the flame structure. The subsequent tendency to level off results from the gradual decrease of flame surface density as the fuel is consumed, as well as the continued entrainment of air into the jet structure. The final decrease in nitric oxide concentration results from the mixing of the existing nitric oxide and additional, non-reacting oxidizer.

The maximum value of P_N attained is about unity, and the physical value of concentration may be estimated using Equation 65. Recalling the calculated values $k = 5.66 \times 10^{-4}$ sec^{-1} and $\beta_1 = 0.142$, we find that the actual concentration is

$$\Phi_N \cong 4.0 \times 10^{-3} \left(\frac{d}{W_0}\right) P_N \qquad (77)$$

so that for a one foot diameter burner with an efflux velocity of 100 feet/second, $\Phi_N \cong 4.0 \times 10^{-5}$ or 40 parts per million.

The results of a corresponding calculation are shown in Figure 4 for the model in which the laminar diffusion flame calculations are based upon the local mean reactant concentrations rather than upon the uncontaminated values. The results consequently account for the lower reactant consumption rate per unit flame area, the greater flame surface density which

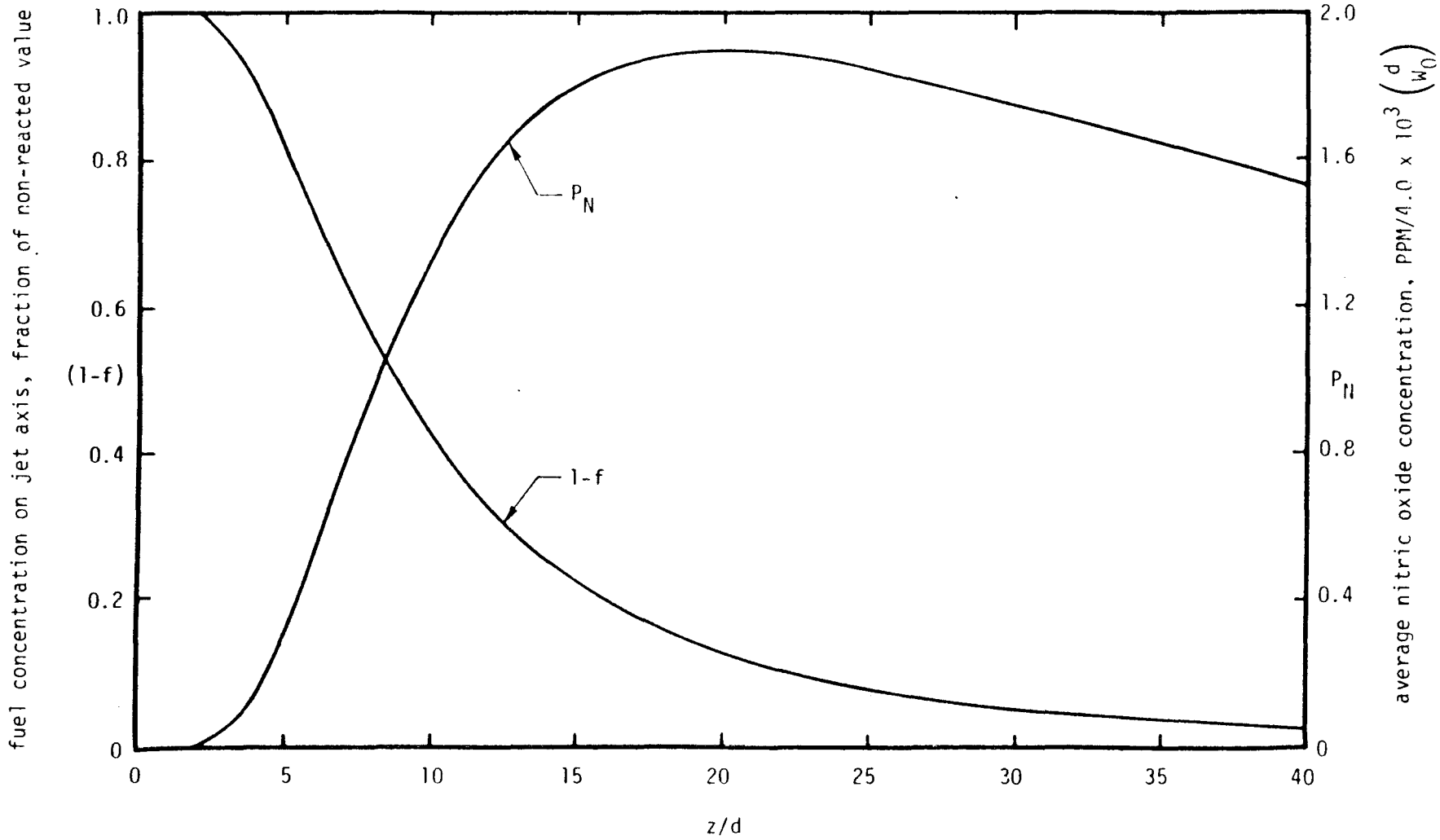

Figure 4. Fuel concentration on jet axis and integrated nitric oxide concentration. Methane-air flame; detailed reaction kinetics and reaction dilution with reaction products.

develops as a consequence and the greater production of nitric oxide. This system is defined by the differential equations, Equations 71 and 72, and the more complicated coefficients given by Equations 74, 75, and 76. Again, the production of nitric oxide is described by the differential equation, Equation 66.

The fuel concentration, as appears by comparison of the two figures, is not strongly affected by the inclusion of reactant vitiation so far as either the length of the flame or the concentration distribution is concerned. This result illustrates very well the manner in which fuel consumption rate by a flame element and the total flame surface area within the jet envelope, compensate so that this product is essentially constant. The nitric oxide production, however, responds nearly proportionally to the flame surface density and, as a consequence, is higher for the flame structure that accounts for vitiation. In this case, the nitric oxide production is nearly doubled from jet calculations utilizing uncontaminated reactants.

The scaling law for nitric oxide production is contained in Equation 65:

$$\Phi_N = \frac{1}{\beta_1} \frac{\ell\, d}{W_0} P_N \tag{78}$$

in which β_1 and ℓ are constants and P_N is independent of the fuel jet diameter and velocity. The prediction, then, is that the nitric oxide concentration at the end of the flame varies linearly with diameter and inversely with the jet velocity.

Sufficient experimental data is not yet available for critical comparison with the predicted nitric oxide concentration values or with the scaling law. The observed levels, however, are considerably higher than those given by Equation 78 and appear to have a weaker dependence on jet diameter than this equation predicts. The difference in concentration level may come from the reactions, neglected in the analysis, which take place in the burned-off portions of the flame. The extension of the model described in the next section is intended to account for these additional reactions.

XI. AN EXTENSION OF THE COHERENT FLAME MODEL

The coherent flame model, as originally formulated and as applied in the preceding sections, assumes that chemical reaction rates are fast relative to mixing rates. This section outlines an extension of the model which allows both fast and slow reactions to be treated. The motivation for such an extension is the need for a description of the nitric oxide production which occurs in the methane-air flame after the more rapid energy producing reactions are complete.

In the model, as applied in Sections VI and VII, all reactions take place in the strained laminar flame. When these are all fast, the species consumption and production rates are equal to the rate per unit flame area multiplied by the flame area per unit volume. That is, there are no further reactions in the products generated when portions of the flame sheet burn off in the flame shortening process. Reactions that are slow, however, such as those which lead to nitric oxide, may continue in such regions. It is the purpose of the model extension to account for these additional reactions.

It is clear that for a kinetic system of any complexity, such as that for methane-air, the reactions taking place in the product gases must be treated numerically as they are presently in the strained flame. Such a requirement necessitates a simplification in some aspects of the model if the computational effort is to remain reasonable. A somewhat different view of the turbulent mixing process, about which there is some disagreement (even between the present authors), appears to provide sufficient simplification. The approach is suggested by the many experiments on mixing layers, for example, those of Brown and Roshko[4] and Konrad[5], and, more recently,

on turbulent jets,[6] which may be interpreted to imply that it is in the breakdown of large-scale structures that molecular mixing and the subsequent chemical reactions occur, i.e., that the reactants are entrained into the layer and jet by large inviscid motions and subsequently mix as the large structure breaks down. If this interpretation is correct, it suggests the approximation that mean quantities be taken as independent of the transverse, y, or radial, r, direction and that attention be concentrated on the axial (or, in a sense, temporal) variations. We assume then that, in both the mixing layer and the axisymmetric jet, the mean quantities, velocity, concentration, flame surface density, and so forth, depend only on the axial dimension, x.

With the above simplifications in mind, the model extension may be described as follows. Within the mixing layer or jet, the reactants are divided by the flame sheet into two streams: one containing fuel and the other oxidizer. The reaction between fuel and oxidizer, being fast, occurs only within the flame sheet. The slow reactions, those resulting in NO for instance, take place both within the flame sheet and in the two fluid streams. The chemical constitution of the two bulk fluids is determined by four processes: (1) the volume reactions, (2) the continuous addition to them of the products of the flame sheet reactions that occurs during flame shortening, (3) the addition of newly-entrained fuel and oxidizer, and (4) the removal of reactants entering the flame sheet. (In the fuel jet, only the oxidizer fluid is continuously replenished by new reservoir gas.) The mass rate with which flame sheet products are added to the bulk gas is to be put equal to the flame shortening rate multiplied by the flame mass per unit area. This latter quantity, as well as the composition, is given by the strained flame structure calculation. The division of these products between fuel and oxidizer streams is a required input to the model. The calculations of Sections VI and VII and experimental data will serve as guides in choosing this parameter. If the reaction rates can be divided into two groups, one fast and the other slow relative to mixing rates, then to a good approximation, the bulk fluids are homogeneous and the reactions can be described by standard kinetic codes modified to allow for the above described addition and removal of reactants.

With the fuel and oxidizer gas composition known and the strain rate determined by the local fluid mechanics, the strained flame computation can be made as before. What is needed, therefore, are simultaneous, coupled computations of the reactions within the bulk fluid, the strained flame reactions, and the flame shortening rate.

The equation governing the flame surface area is the same as that in the original model. For the mixing layer of width y, the expression is

$$U \frac{d}{dx} (y \Sigma) = \alpha \epsilon \Sigma y - \lambda \left[v_1 \Sigma^2/\kappa_1 + v_2 \Sigma^2/\kappa_2 \right] y$$

This equation, the stream tube, and the strained flame equations are to be solved simultaneously for the variation of the chemical properties with x.

With regard to the strained flame calculation, the strain rate and stream compositions vary slowly compared to the flow times within the flame. The calculation, therefore, may be viewed as a quasi-steady one with the properties within the flame changing instantaneously with change in the bulk fluid state. It may not be necessary to make this computation at each axial station. The results described in Section V suggest the possibility of interpolation between a few such stations.

As the above described calculation proceeds step by step in the axial direction, the change in flux of each chemical species in the mixing layer, for example, is given by the equation

$$U \frac{d(\text{flux})_i}{dx} = \alpha_1 U_1 \kappa_i(\infty) + \alpha_2 U_2 \kappa_i(-\infty) + v_i \Sigma y + \dot{\Omega}_{i,f} + \dot{\Omega}_{i,0}$$

in which $(\text{flux})_i$ is the total flux of species i, (∞) and $(-\infty)$ refer to the fuel and oxidizer streams, and the $\dot{\Omega}$'s are the total production rates in the bulk streams. The other symbols are defined in Figure 15 or have the meanings given in the earlier sections.

It is recognized that this brief sketch leaves many details unclear. Some have been omitted to simplify the discussion, but others remain to be worked out. It is hoped, however, that the physical picture on which the model is to be constructed has been adequately described.

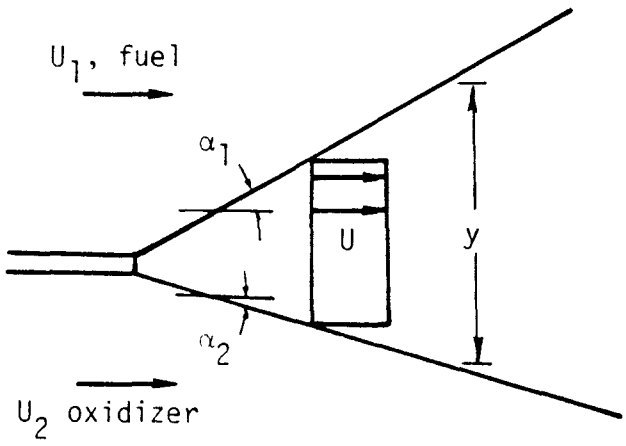

Figure 5. The two-dimensional mixing layer

XII. CONCLUDING REMARKS

As was implied by the remarks at the end of Section VII, more experimental data is needed on the production of nitric oxide in methane-air flames, particularly of different scale, before a critical assessment can be made of the present analysis. The theoretical results already obtained, however, suggest the usefulness of a further application and development of the model.

XIII. REFERENCES

1. Marble, F. E. and Broadwell, J. E., "The Coherent Flame Model for Turbulent Chemical Reactions," Project SQUID Technical Report No. TRW-9-PU, January 1977.

2. Batchelor, G. K., "The Effect of Homogeneous Turbulence on Material Lines and Surfaces," Proc. Roy. Soc. A213, p. 349.

3. Hawthorne, W. R., Weddell, D. S., and Hottel, H. C., "Mixing and Combustion in Turbulent Gas Jets," Proceedings Third Symposium on Combustion, Flame, and Explosion Phenomena, p. 266 (1948). Williams and Wilkens Co., Baltimore, Md.

4. Brown, G. and Roshko, A., "On Density Effects and Large Structure in Turbulent Mixing Layers," J. Fluid Mech. 64, pp. 775-816.

5. Konrad, J. H., "An Experimental Investigation of Mixing in Two-Dimensional Turbulent Shear Flows with Applications to Diffusion-Limited Chemical Reactions." Project SQUID, Purdue Univ., Indiana, Technical Report CIT-8-PU.

6. Dimotakis, P. ••• private communication.

XIV. APPENDIX A

LAMINAR DIFFUSION FLAMES WITH FAST CHEMICAL KINETICS

The reactant consumption rates enter into the problem in the form v_1 and v_2, the volumes of fuel and oxidizer consumed per unit flame area, respectively, and play roles both in the species conservation relations and in the equations describing the flame surface density. These quantities are assumed to be determined locally by the flame structure and to depend only upon local quantities; in particular, for the diffusion flame, they are determined by fuel and oxidizer concentrations and a local fluid mechanical property. As shall be illustrated, they may be determined analytically when the kinetics are fast. The important point to keep in mind is that the entire flame structure and chemical kinetics are coupled with the field analysis rather weakly, so that the consideration of complex kinetics complicates only the local flame structure and not the formulation of the flowfield and the flame distribution.

As the first example, consider the diffusion flame with rapid kinetics; in this approximation the reaction takes place at a surface of infinitesimal thickness. Utilizing the coordinates x and y to signify distances parallel to and normal to the flame surface, supposed to lie along y = 0, the fuel and oxidizer concentrations satisfy the equations

$$\frac{\partial \kappa_1}{\partial t} + u \frac{\partial \kappa_1}{\partial x} + v \frac{\partial \kappa_1}{\partial y} = \frac{1}{\rho} \frac{\partial}{\partial y} \left(\rho D \frac{\partial \kappa_1}{\partial y} \right) \tag{A1}$$

$$\frac{\partial \kappa_2}{\partial t} + u \frac{\partial \kappa_2}{\partial x} + v \frac{\partial \kappa_2}{\partial y} = \frac{1}{\rho} \frac{\partial}{\partial y} \left(\rho D \frac{\partial \kappa_2}{\partial y} \right) \tag{A2}$$

where

$$\frac{\partial u}{\partial x} + \frac{\partial v}{\partial y} = 0 \tag{A3}$$

when the heat of reaction is negligible and the gas density ρ is a constant. For the classical diffusion flame, the field is independent of x, but the solution is time dependent. Then, since $\frac{\partial u}{\partial x} = 0$, $v = v(t)$ which, as will appear, is not generally zero. Then introducing the variable

$$\zeta = \frac{y}{\sqrt{Dt}} \tag{A4}$$

and taking

$$v(t) = \Lambda\sqrt{\frac{D}{t}} \tag{A5}$$

the species conservation equations are reduced to a similarity form and become

$$\frac{d^2\kappa_i}{d\zeta^2} + \left(\frac{\zeta}{2} - \Lambda\right)\frac{d\kappa_i}{d\zeta} = 0 \tag{A6}$$

where i = 1, 2 for fuel or oxidizer, respectively. This pair of differential equations is required to satisfy the conditions that the fuel and oxidizer mass fractions take on the values $\kappa_1(\infty)$ and $\kappa_2(-\infty)$ at $y = +\infty$ and $y = -\infty$, respectively and that the mass flux to the diffusion flame, $y = 0$, supplies fuel and oxidizer in the stoichiometric ratio. This latter condition is explicitly

$$\frac{\rho D \frac{\partial \kappa_1}{\partial y}(0,t)}{-\rho D \frac{\partial \kappa_2}{\partial y}(0,t)} = f \tag{A7}$$

where f is the known, constant stoichiometric fuel-oxidizer ratio. It is not difficult to show that the appropriate solution is

$$\kappa_1 = \kappa_1(\infty)\,\frac{\operatorname{erf}\left(\frac{\zeta}{2} - \Lambda\right) + \operatorname{erf}(\Lambda)}{1 + \operatorname{erf}(\Lambda)} \tag{A8}$$

and

$$\kappa_2 = \kappa_2(-\infty)\,\frac{\operatorname{erf}\left(-\frac{\zeta}{2} + \Lambda\right) - \operatorname{erf}(\Lambda)}{1 - \operatorname{erf}(\Lambda)} \tag{A9}$$

satisfying the differential Equation (A6) and the boundary conditions at $y = \pm\infty$. The stoichiometry condition (Equation A7) then determines the characteristic value Λ, and it is a matter of calculation to show that this

gives the result

$$\frac{\kappa_1(\infty)\ [1 - \text{erf}\ (\Lambda)]}{\kappa_2(-\infty)[1 + \text{erf}\ (\Lambda)]} = f \tag{A10}$$

Now $\kappa_1(\infty)/\kappa_2(-\infty)$ is the imposed fuel-oxidizer ratio of the problem, and the quotient of this with the stoichiometric fuel-oxidizer ratio

$$\frac{\kappa_1(\infty)/\kappa_2(-\infty)}{f} \equiv \phi \tag{A11}$$

is frequently called the equivalence ratio. Thus, the value of Λ becomes

$$\Lambda = \text{erf}^{-1}\left(\frac{\phi - 1}{\phi + 1}\right) \tag{A12}$$

This quantity defines the value of the transverse gas velocity

$$v(t) = \sqrt{\frac{D}{t}}\ \text{erf}^{-1}\left(\frac{\phi - 1}{\phi + 1}\right) \tag{A13}$$

which is required to keep the flame stationary at the x-axis. With this solution, the values of the reactant volume consumption rates may be calculated as

$$v_1 = \kappa_1(\infty)\ \sqrt{\frac{D}{\pi t}}\ \left(\frac{\phi + 1}{2\phi}\right) e^{-\Lambda^2} \tag{A14}$$

and

$$v_2 = \kappa_2(-\infty)\sqrt{\frac{D}{\pi t}}\ \left(\frac{\phi + 1}{2}\right) e^{-\Lambda^2} \tag{A15}$$

This result exhibits the intuitively clear result that the consumption rates decrease with increasing time, because the diffusion layers that supply the reactants grow thicker with time. The equivalence ratio, which determines the value of Λ, is known because $\kappa_1(\infty)$ and $\kappa_2(-\infty)$ are equal to the values remote from the turbulent flame since the diffusion zone thickness is assumed small in comparison with flame front spacing. At any point within the turbulent flame, therefore, the reactant consumption rates are known in terms of the time t elapsed since the formation of the flame.

In discussing the turbulent flame structure it was emphasized that the turbulent motions tend to extend the flame surface and that the significant part of this extension consists of strain rate in the plane of the flame. Now, if the flame is aligned with the x-axis and the remaining axes chosen so that straining rate is along the x-axis, the resulting strained diffusion flame is also directly soluble. In the particular instance when the straining rate in the fluid is large, i.e., where

$$\varepsilon \equiv \frac{\partial u}{\partial x} \tag{A16}$$

is large and constant, Equations (A1) through (A3) take the form

$$\frac{\partial \kappa_i}{\partial t} + v \frac{\partial \kappa_i}{\partial y} = \frac{\partial}{\partial y}\left(D \frac{\partial \kappa_i}{\partial y}\right) \tag{A17}$$

and

$$\varepsilon + \frac{\partial v}{\partial y} = 0 \tag{A18}$$

If we solve the problem as previously posed, the solution has a brief transient followed by a steady solution which we may obtain be neglecting $\partial \kappa_i / \partial t$ and taking v and κ_i to be functions of y only. Then introducing the variable

$$\zeta \equiv \frac{y}{\sqrt{D/2}} \tag{A19}$$

$$v = -\varepsilon y + \sqrt{2\varepsilon D}\ \Lambda \tag{A20}$$

with Λ unknown, the differential equation (A17) becomes

$$\frac{d^2 \kappa_i}{d\kappa^2} + \left(\frac{\zeta}{2} - \Lambda\right) \frac{d\kappa_i}{d\zeta} = 0 \tag{A21}$$

formally identical with Equation (A6). The conditions for $y \pm \infty$, as well as stoichiometry condition at the flame front, are also identical with those of the time-dependent flame, and, hence, the solution for the strained

flame is likewise given by Equations (A8) and (A9) together with Λ evaluated by Equation (A12), but with ζ as defined in Equation (A19). The corresponding volume consumption rates of reactants are easily calculated

$$v_1 = \kappa_1(\infty) \sqrt{\frac{D\varepsilon}{2\pi}} \left(\frac{\phi + 1}{\phi}\right) e^{-\Lambda^2} \tag{A22}$$

and

$$v_2 = \kappa_2(-\infty) \sqrt{\frac{D\varepsilon}{2\pi}} \left(\phi + 1\right) e^{-\Lambda^2} \tag{A23}$$

Thus, so far as the local flame structure is concerned, the features relevant to the turbulent flame calculation are determined by the local strain rate.

X. APPENDIX B

TEMPERATURE AND CONCENTRATION PROFILES FOR STRAINED LAMINAR METHANE-AIR FLAMES

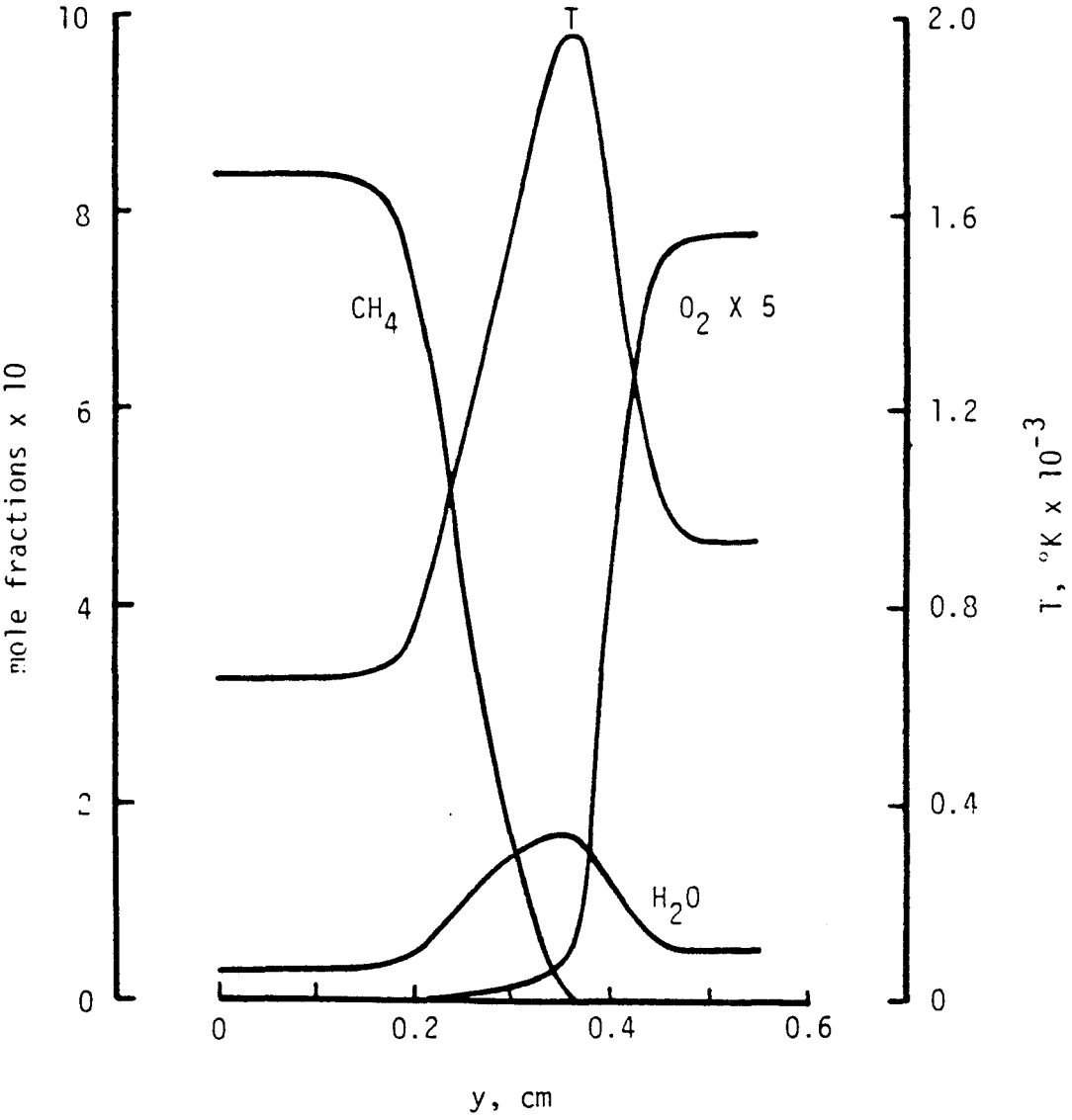

Figure B-1. Temperature, CH_4, O_2, and H_2O distributions in strained laminar methane-air flame; $\varepsilon = 600\ sec^{-1}$, $\kappa_1 = \kappa_2 = 0.75$.

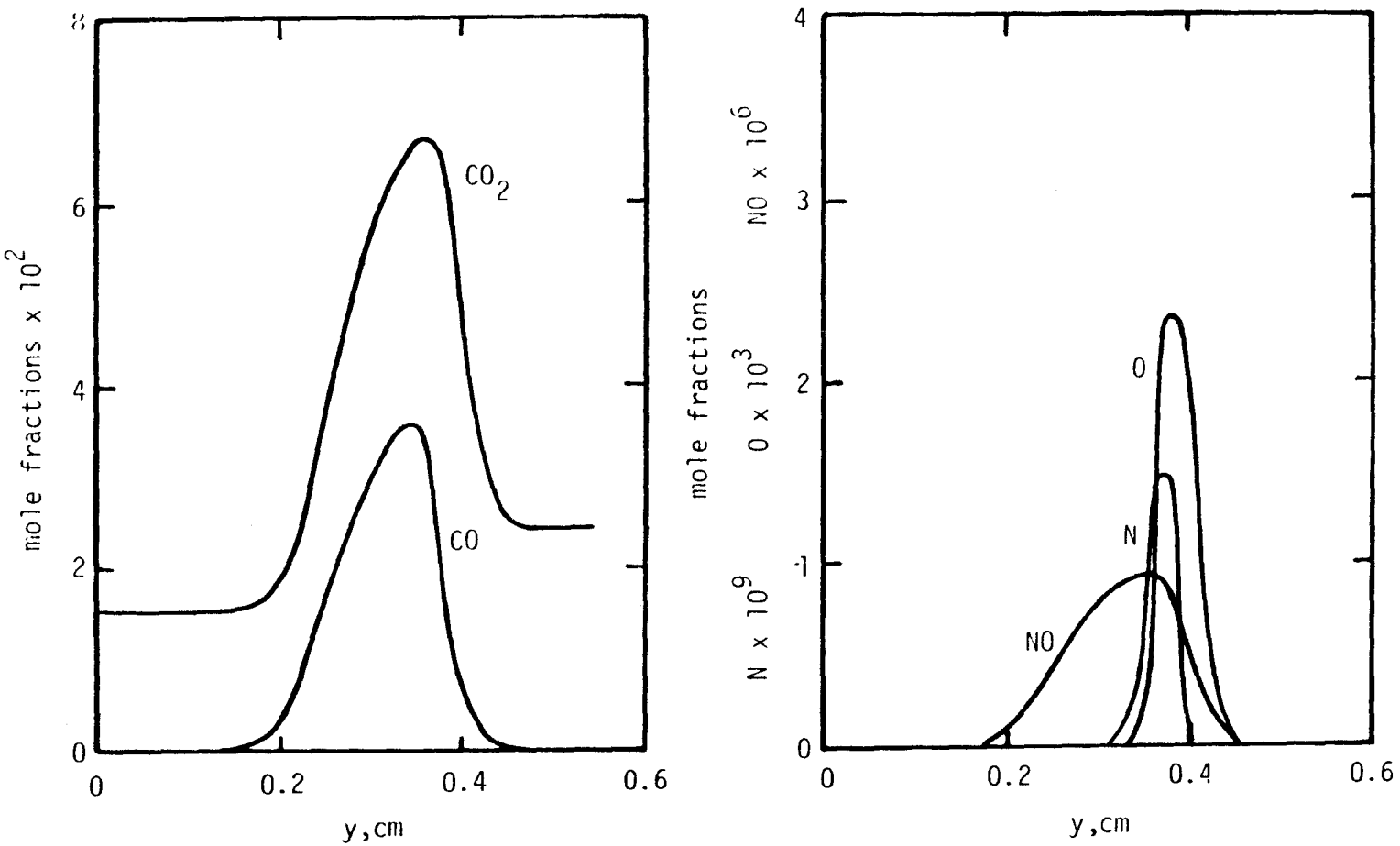

Figure B-2. CO_2, CO, O, N, and NO distributions in strained laminar methane-air flame; ε = 600 sec^{-1}, $\kappa_1 = \kappa_2 = 0.75$.

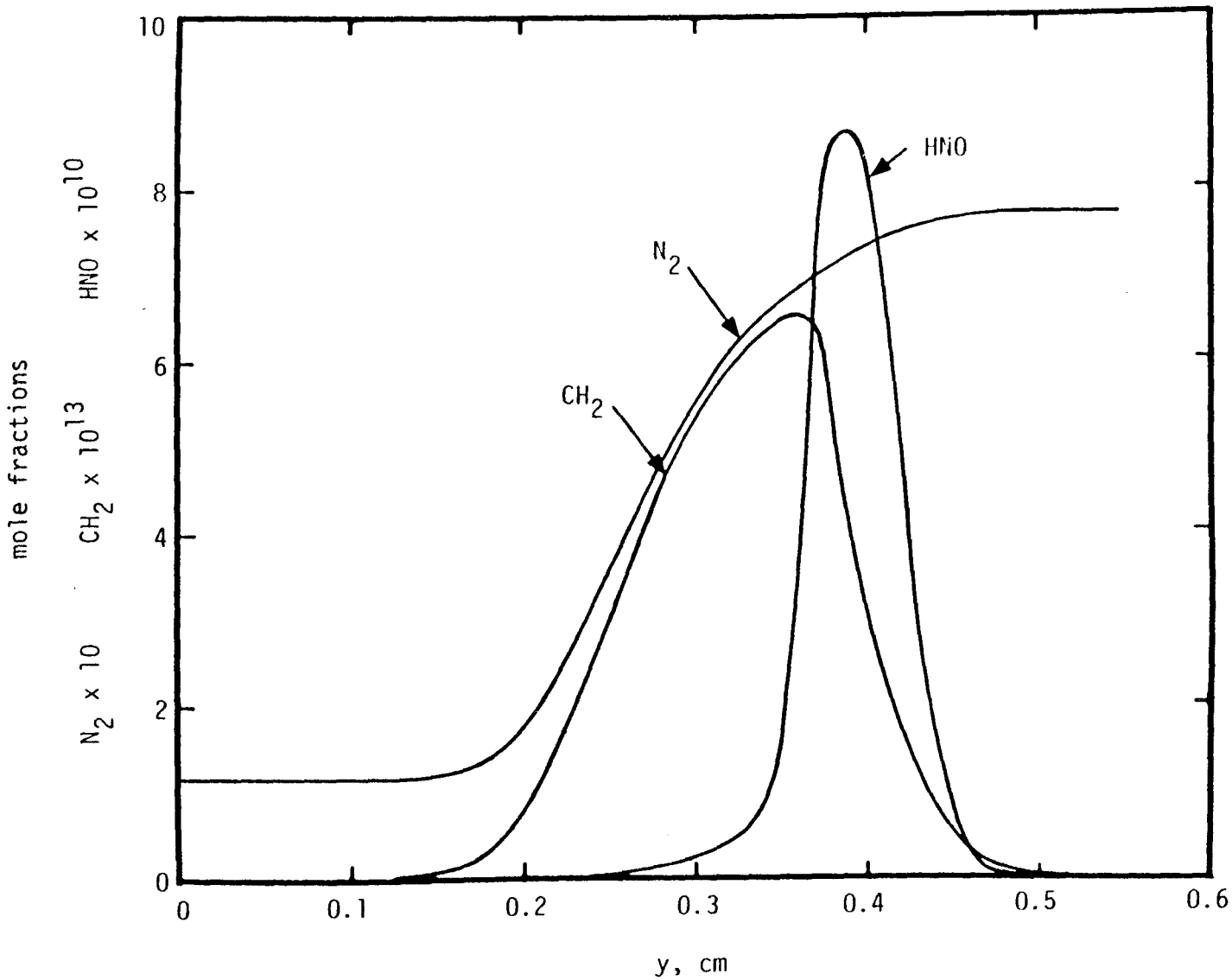

Figure B-3. CH_2, N_2, and HNO distributions in strained laminar methane-air flame; $\varepsilon = 600\ sec^{-1}$, $\kappa_1 = \kappa_2 = 0.75$.

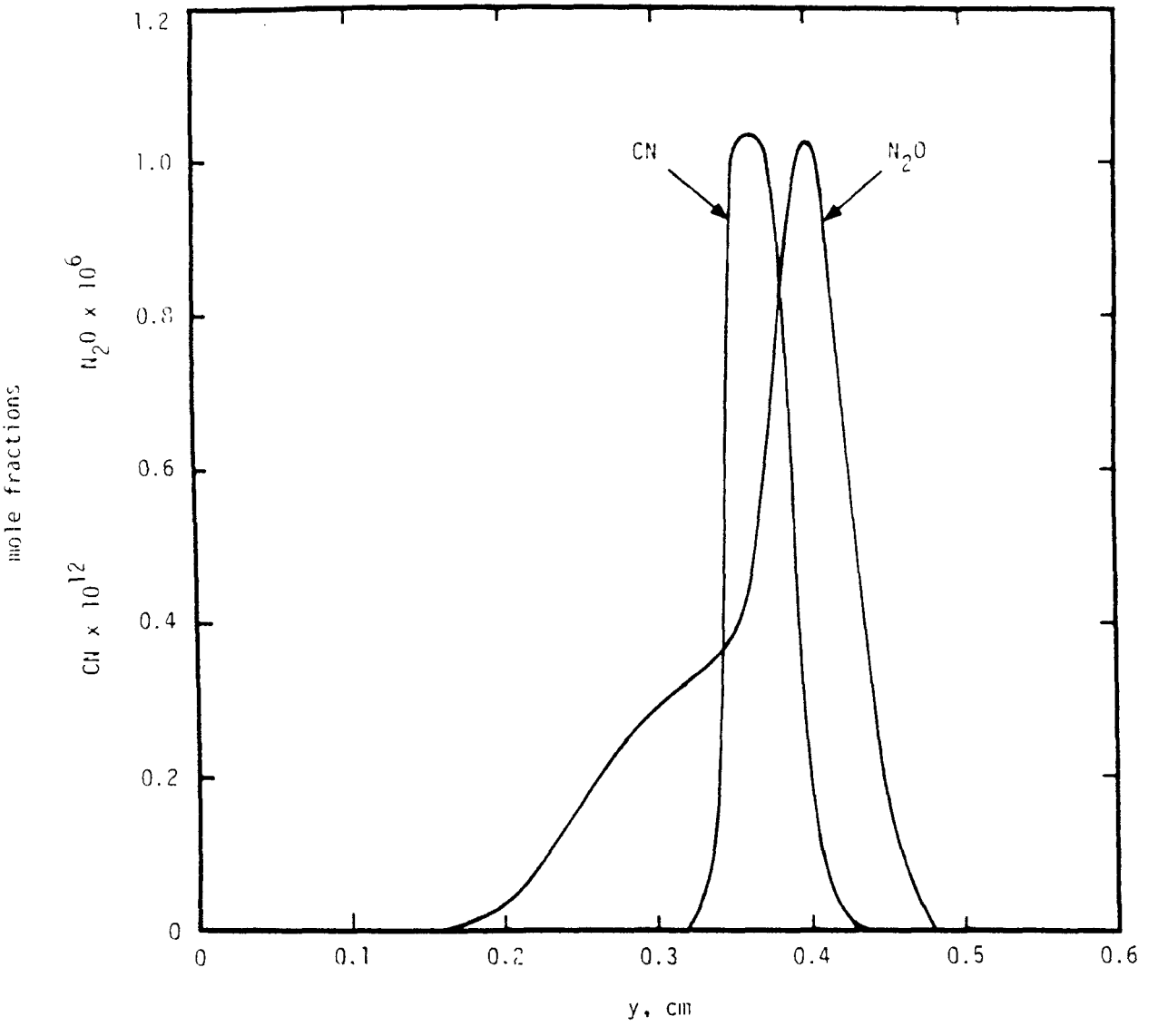

Figure B-4. CN and N_2O distributions in strained laminar methane-air flame; ε = 600 sec^{-1}, $\kappa_1 = \kappa_2 = 0.75$.

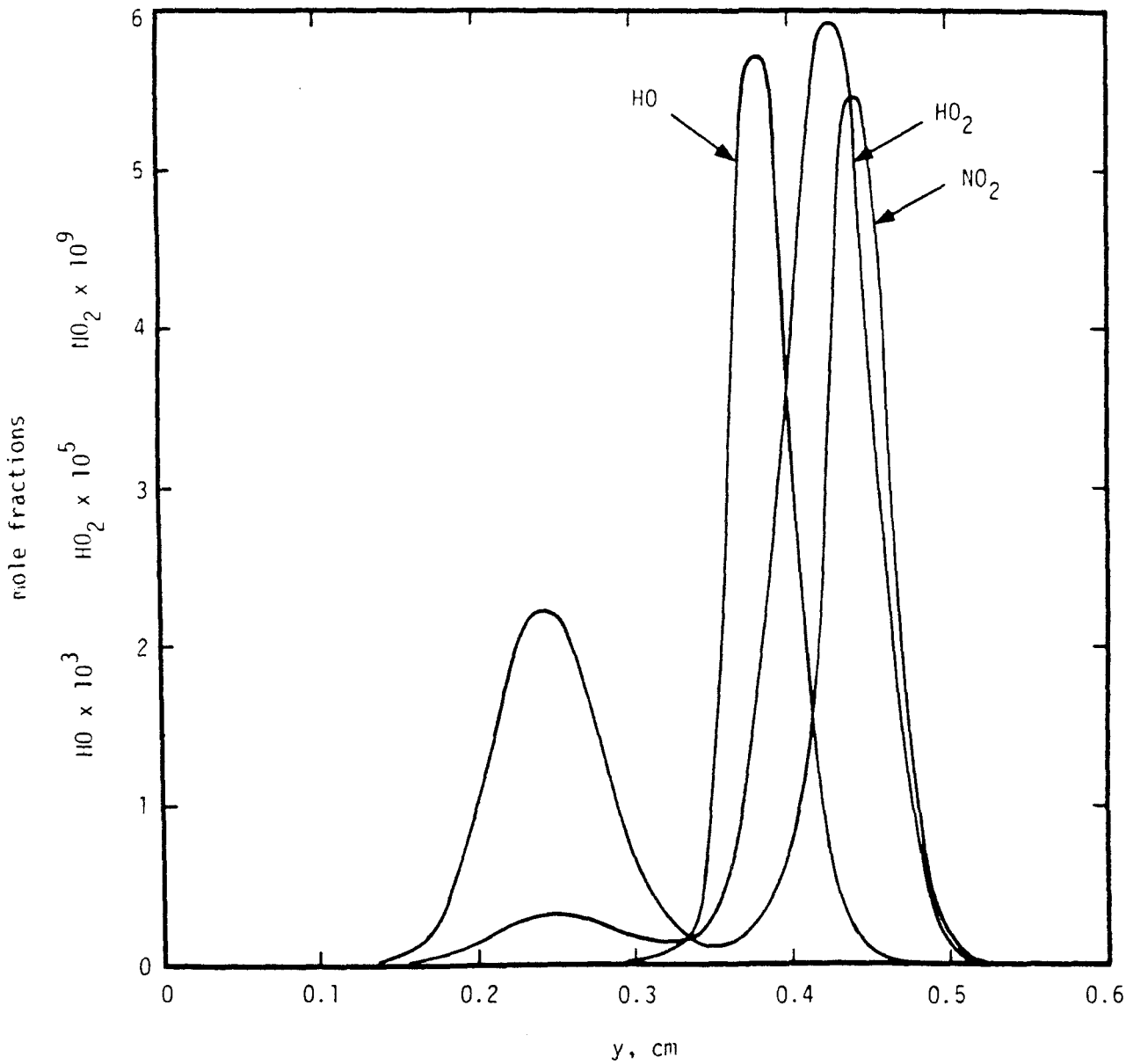

Figure B-5. HO, HO_2, and NO_2 distributions in strained laminar methane-air flame; ε = 600 sec^{-1}, $\kappa_1 = \kappa_2 = 0.75$.

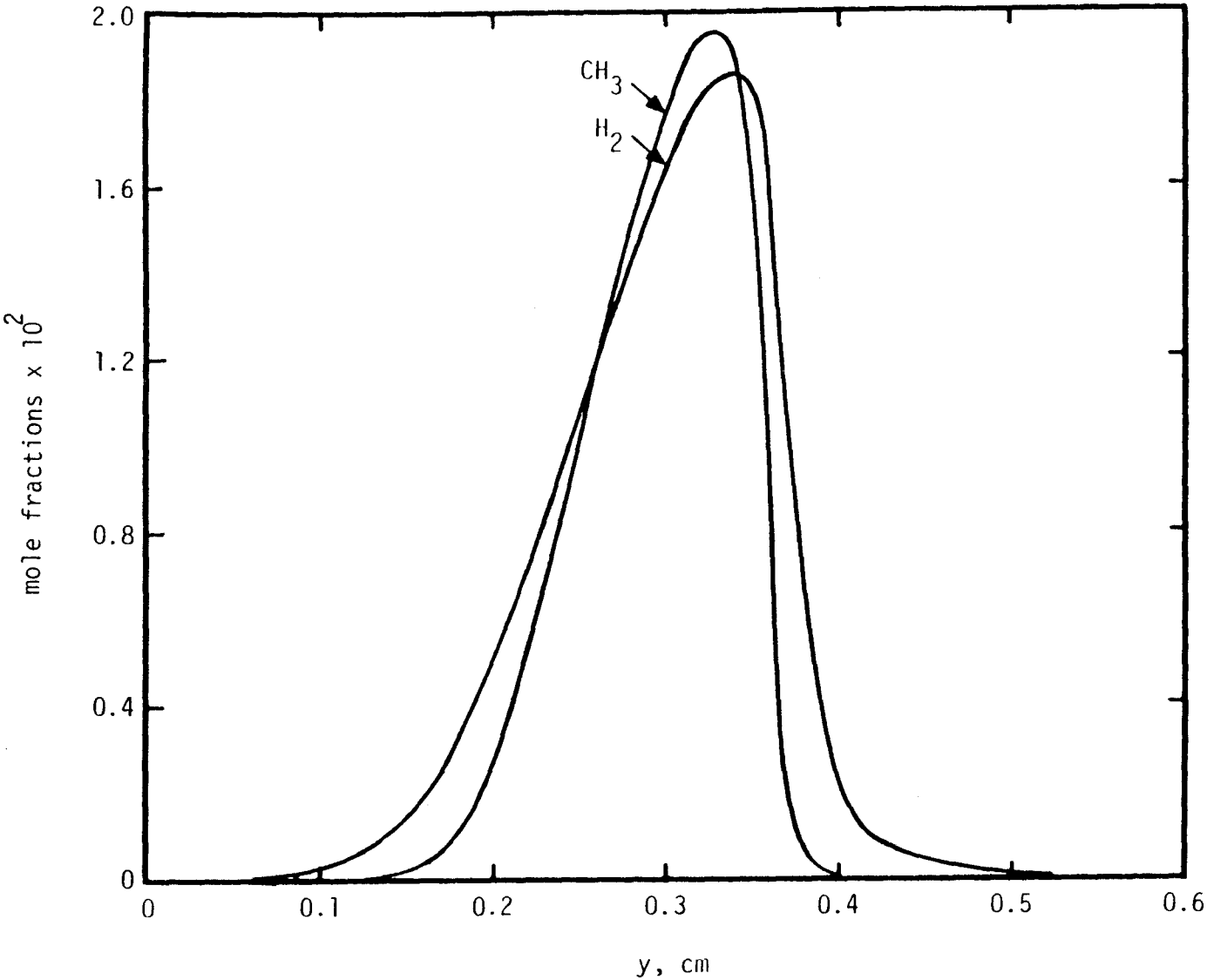

Figure B-6. CH_3 and H_2 distributions in strained laminar methane-air flame, ε = 600 sec^{-1}, $\kappa_1 = \kappa_2 = 0.75$.

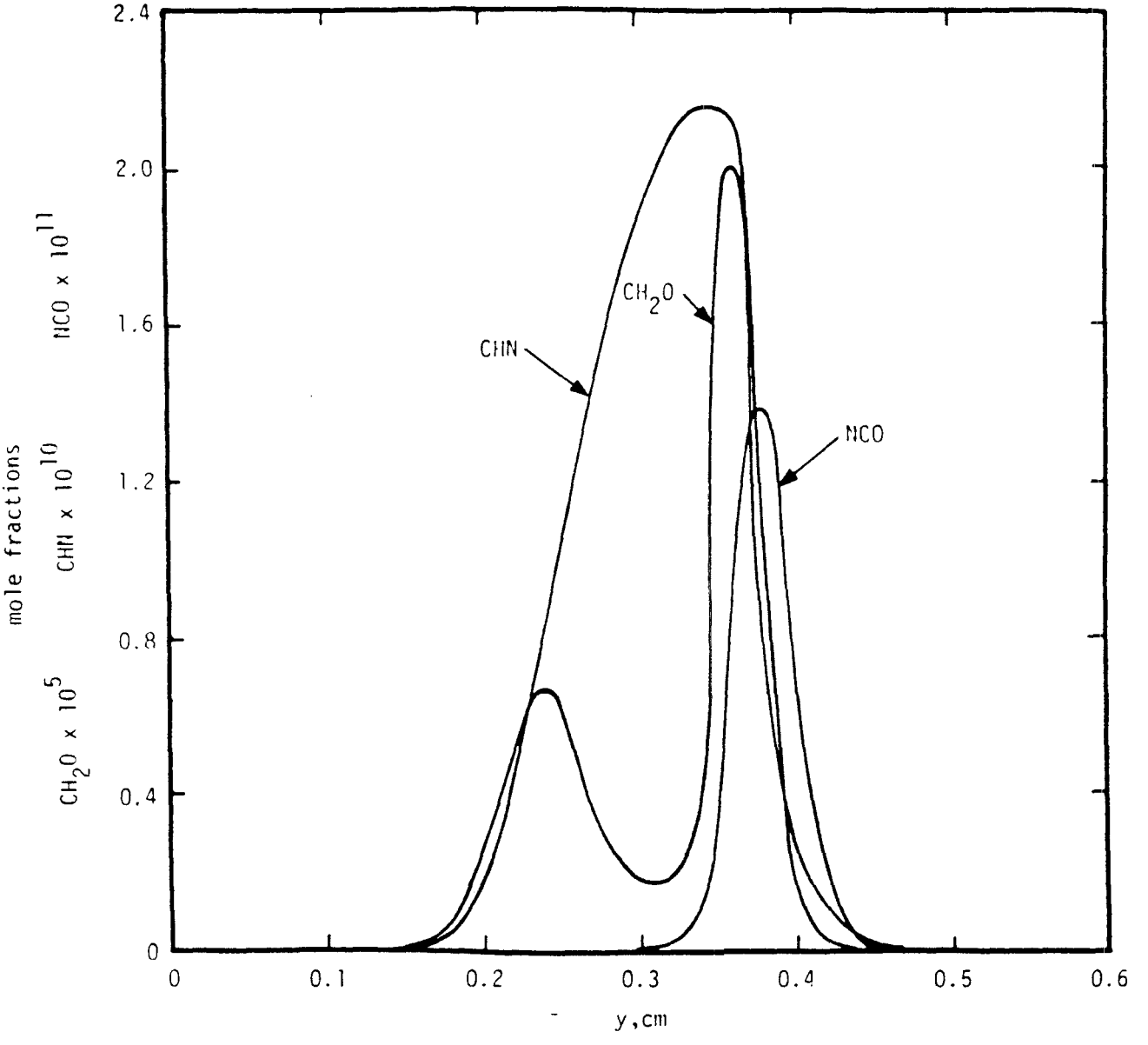

Figure B-7. CHN, CH_2O, and NCO distributions in strained laminar methane-air flame; ε = 600 sec^{-1}, $\kappa_1 = \kappa_2 = 0.75$.

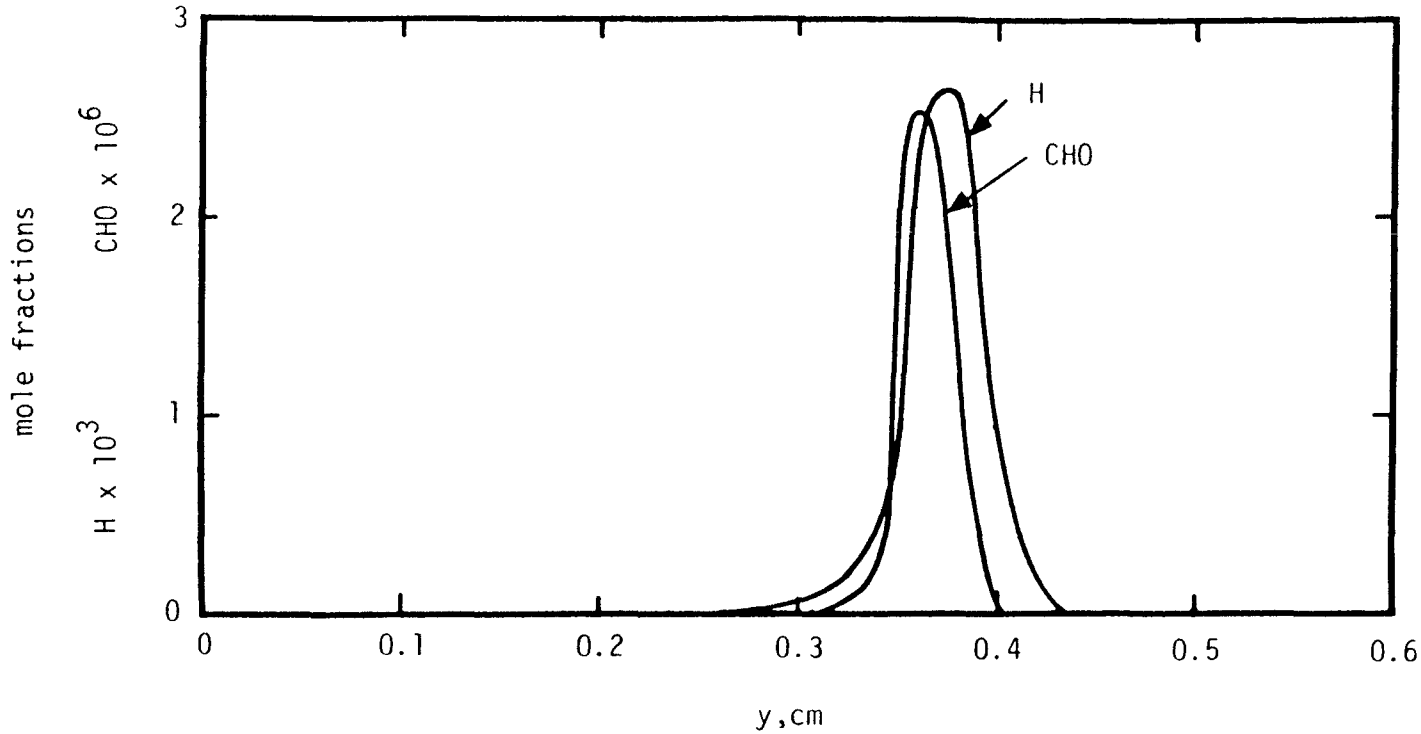

Figure B-8. H and CHO distributions in strained laminar methane-air flame; ε = 600 sec^{-1}, $\kappa_1 = \kappa_2 = 0.75$.

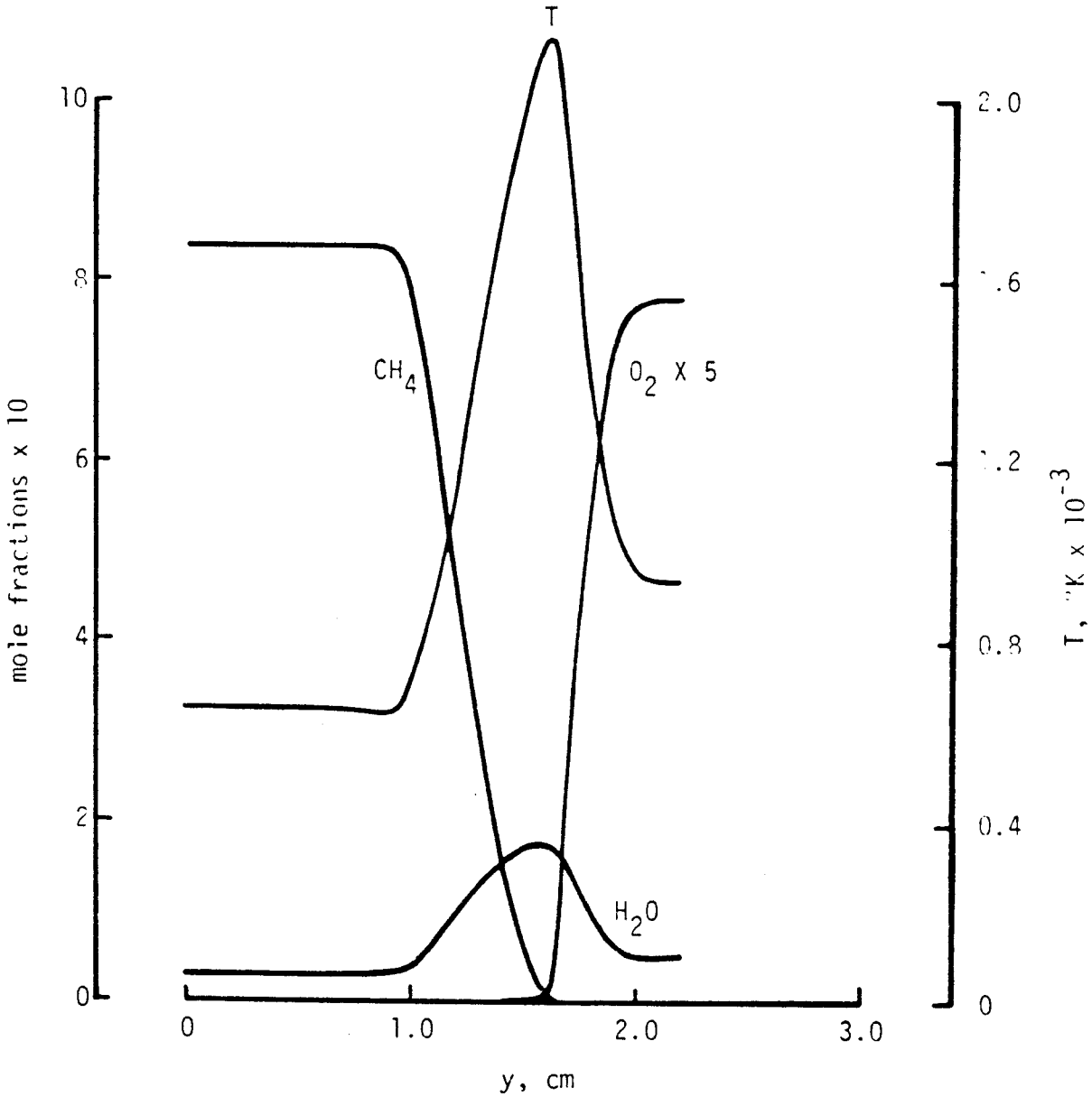

Figure B-9. Temperature, CH_4, O_2, and H_2O distributions in strained laminar methane-air flame; $\varepsilon = 50\ sec^{-1}$, $\kappa_1 = \kappa_2 = 0.75$.

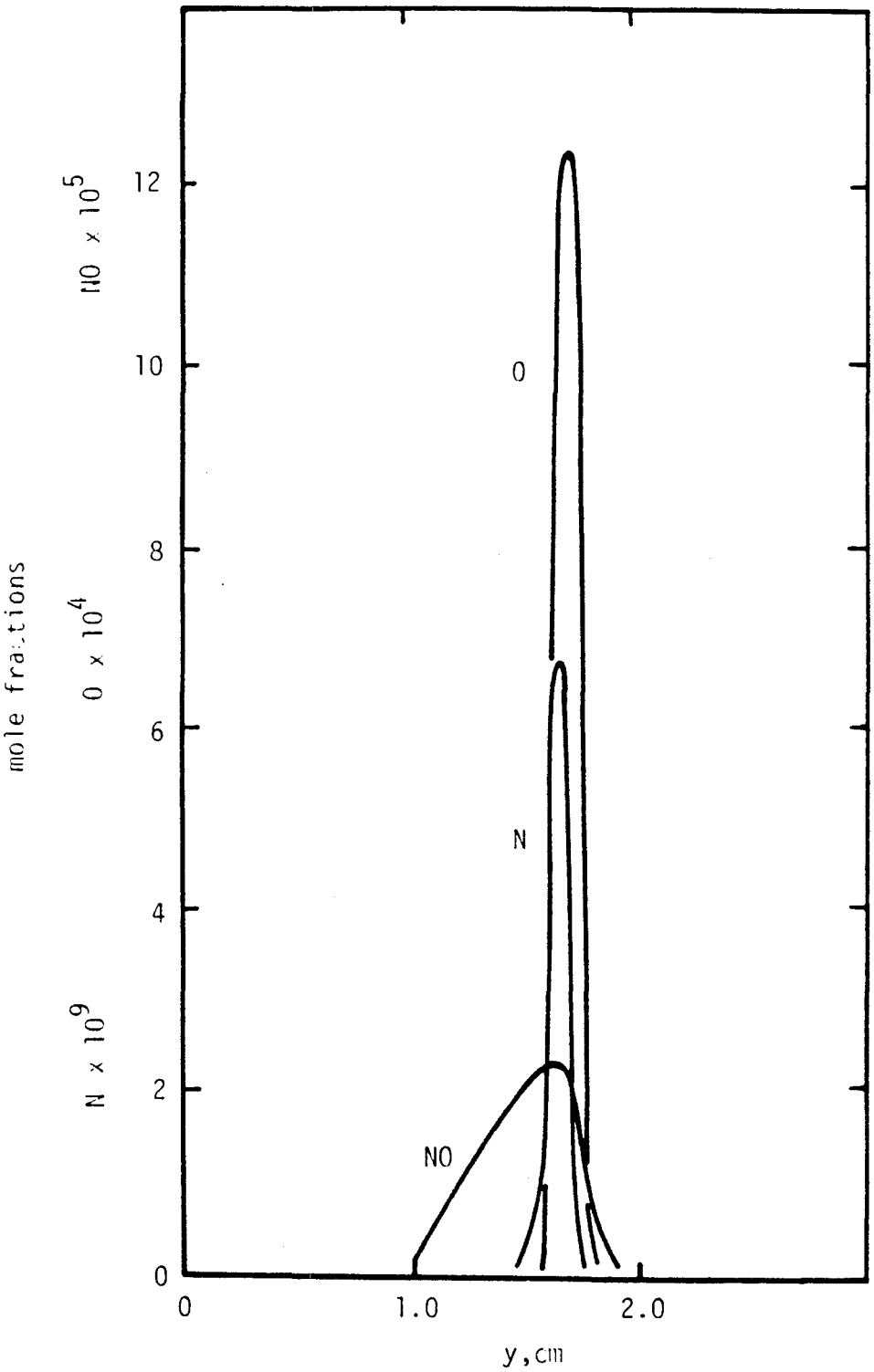

Figure B-10. O, N, and NO distributions in strained laminar methane-air flame; $\varepsilon = 50\ sec^{-1}$, $\kappa_1 = \kappa_2 = 0.75$.

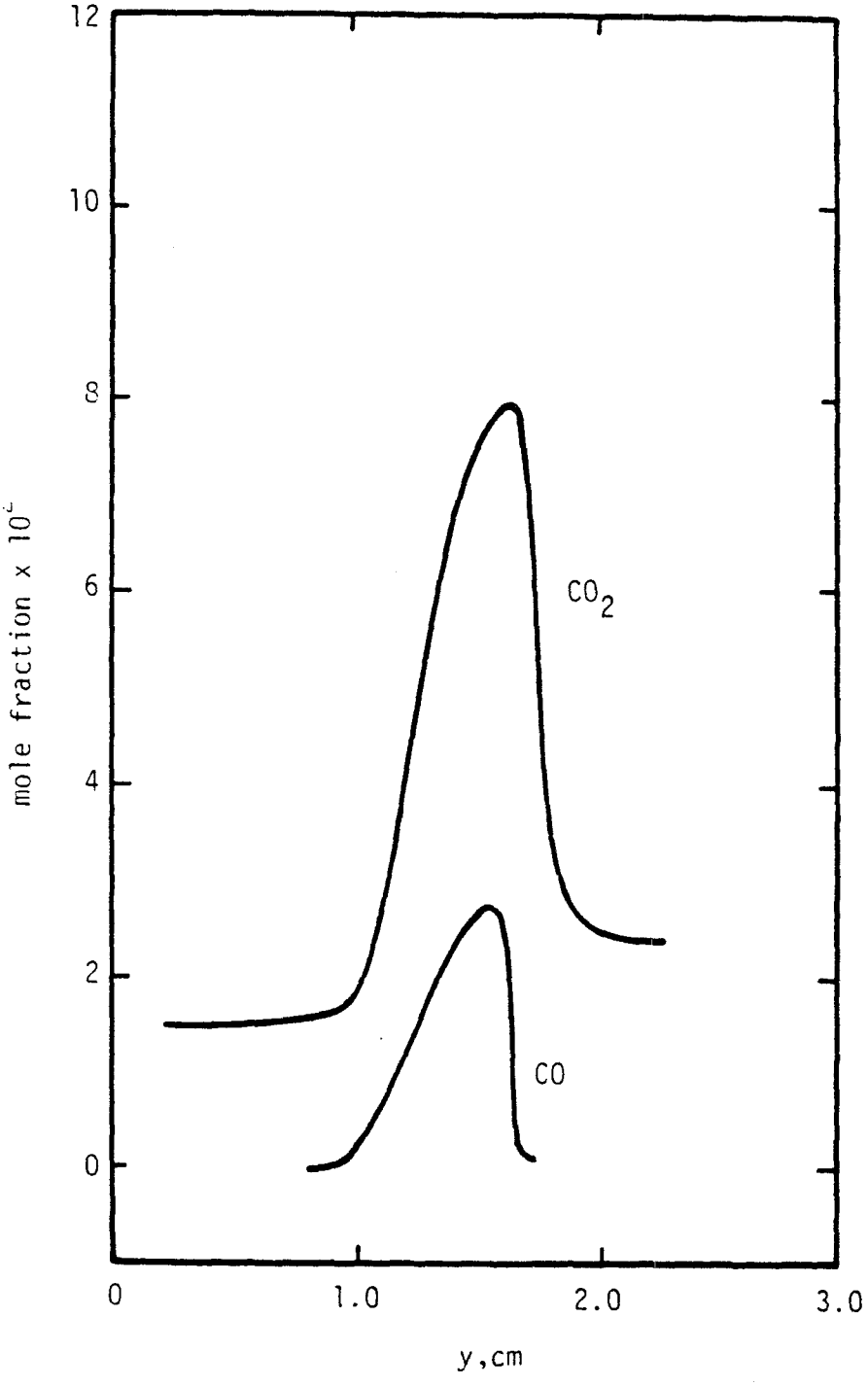

Figure B-11. CO_2 and CO distributions in strained laminar methane-air flame; ε = 50 sec^{-1}, $\kappa_1 = \kappa_2 = 0.75$.

TECHNICAL REPORT DATA
(Please read Instructions on the reverse before completing)

1. REPORT NO.	2.	3. RECIPIENT'S ACCESSION NO.
EPA-600/7-80-018		

4. TITLE AND SUBTITLE	5. REPORT DATE
A Theoretical Analysis of Nitric Oxide Production in a Methane/Air Turbulent Diffusion Flame	January 1980
	6. PERFORMING ORGANIZATION CODE

7. AUTHOR(S)	8. PERFORMING ORGANIZATION REPORT NO.
Frank E. Marble (California Institute of Technology) and James E. Broadwell	

9. PERFORMING ORGANIZATION NAME AND ADDRESS	10. PROGRAM ELEMENT NO.
TRW Defense and Space Systems Group One Space Park Redondo Beach, California 90278	INE829
	11. CONTRACT/GRANT NO.
	68-02-2613

12. SPONSORING AGENCY NAME AND ADDRESS	13. TYPE OF REPORT AND PERIOD COVERED
EPA, Office of Research and Development Industrial Environmental Research Laboratory Research Triangle Park, NC 27711	Final: 1/78 - 4/79
	14. SPONSORING AGENCY CODE
	EPA/600/13

15. SUPPLEMENTARY NOTES IERL-RTP project officer is W.S. Lanier, Mail Drop 65, 919/541-2432.

16. ABSTRACT

The report gives results of a theoretical analysis of nitric oxide production in a methane/air turbulent diffusion flame. In the coherent flame model used, the chemical reactions take place in laminar flame elements which are lengthened by the turbulent fluid motion and shortened when adjacent flame segments consume intervening reactant. The rates with which methane and air are consumed and nitric oxide generated in the strained laminar flame are computed numerically in an independent calculation. The model predicts nitric oxide levels of approximately 80 ppm at the end of the flame generated by a 30.5 cm (1 ft) diameter jet of methane issuing at 3050 cm/sec (100 ft/sec). This level varies directly with the fuel jet diameter and inversely with the jet velocity. A possibly important nitric oxide production mechanism, neglected in the analysis, can be treated in a proposed extension to the model.

17. KEY WORDS AND DOCUMENT ANALYSIS

a. DESCRIPTORS		b. IDENTIFIERS/OPEN ENDED TERMS	c. COSATI Field Group	
Pollution	Diffusion Flames	Pollution Control	13B	
Combustion	Mathematical Models	Stationary Sources	21B	12A
Nitrogen Oxide (NO)	Methane	NOx Control	07B	07C
Turbulence		Coherent Structures	20D	
Coherence		Methane/Air Flames		
Shear Flow				

18. DISTRIBUTION STATEMENT	19. SECURITY CLASS (This Report)	21. NO. OF PAGES
Release to Public	Unclassified	69
	20. SECURITY CLASS (This page)	22. PRICE
	Unclassified	

EPA Form 2220-1 (9-73)